Applied Thermal Engineering 202 (2022) 117801

Contents lists available at ScienceDirect

Applied Thermal Engineering

journal homepage: www.elsevier.com/locate/ate

Research paper

The water cost effect of hybrid-parallel condensing systems in the thermo-economical performance of solar tower plants

M. Fernández-Torrijos *, C. Marugán-Cruz, C. Sobrino, D. Santana

Universidad Carlos III de Madrid, ISE Research Group, Thermal and Fluid Engineering Department, Avda. de la Universidad 30, 28911 Leganés, Madrid, Spain

ARTICLE INFO

Keywords:
Hybrid condensing system
Water consumption
Air-cooled condenser
Wet cooling tower
Concentrating solar energy

ABSTRACT

The importance of considering the water price in the analysis of the impact of dry versus hybrid condensing systems in the thermo economical performance of solar tower plants was demonstrated in this work. The dry condensing system consists of several induced-draft air-cooled condenser cells (ACCs) and the hybrid system consists of a parallel system where the condensing steam is split between the ACCs and a surface steam condenser where circulating water is cooled in a wet mechanical-draft cooling tower. The influence of the operating parameters of either the dry or wet cooling systems on the cooling load and fan power consumption were studied. Then, for a given condensing system (a system with a defined number of installed ACCs units and cooling tower units) and given the dry-air and wet-bulb air temperatures, the operating parameters were optimized to maximize the revenues of the power plant. This optimization depends on the water-to-electricity price ratio R, showing that at low ambient temperature when this ratio increases it is not profitable to turn on the cooling towers since the water cost is not counterbalanced by the higher cycle efficiency obtained with the lower condensation temperature. Finally, the annual operation and the LCOE and NPV of the CSP plant located in Dunhuang were analyzed for both dry and hybrid condensing systems with different number of ACCs and wet towers, showing that the most cost-effective configuration is the 16 ACCs with 3 wet cooling towers for water-to-electricity price ratio $R = 4$ ($/m^3)/($/kWh$_e$) and $R = 5$ ($/m^3)/($/kWh$_e$), but for $R = 10$ ($/m^3)/($/kWh$_e$), the best option is with only 2 wet towers.

1. Introduction

Dry cooling is being adopted as an alternative to wet cooling to reduce water consumption in CSP plants, which are often placed in locations with water scarcity. This is motivated both by the goal of reducing water withdraw and comply with environmental regulations, considering that 94% of water consumption of a CSP plant is used by the cooling tower in parabolic trough plant [1]. However, the drawback of dry cooling is the lower electricity production in comparison with wet cooling, due to the higher condensation temperature of the Rankine cycle, especially in locations with higher temperatures. Moreover, the cost of an air cooled condenser is approximately 1.3 times that of the combination surface condensers plus cooling tower.

Some studies [1,2] have been published comparing the impact of dry versus wet cooling in through plants on energy and economical performance, but less effort has been dedicated to power towers despite the results being very dependent on the type of technology. Plants with higher turbine-inlet temperature, like power towers, will be in general penalized less by an increase in the condensation temperature. Hybrid systems are being studied as a halfway option to reduce water consumption while maintaining energy production. These systems consist of a parallel condensing system where the condensing steam is split between an air-cooled condenser and a steam condenser which circulating water is cooled in a wet cooling tower. The wet side of the condensing system is usually turned off during cold and moderate weather.

Asfand et al. [2] evaluated the water consumption and net power generation of a hybrid cooling system for a parabolic trough CSP plant, concluding that the best configuration in terms of water savings was a series–parallel configuration. In this configuration the steam is condensed in a surface condenser which circulating water is sent to a dry cooling tower and then a fraction of this water is further cooled on a wet cooling tower. However the parallel configuration, which sends part of the circulating water from the condenser to a dry cooling tower and part to a wet cooling tower, performed better in terms of energy generation. In the study the authors highlight that further research including an annual performance and economic analysis considering the electricity and water prices and location would help to select the best configuration.

* Corresponding author.
E-mail address: ftorrijo@ing.uc3m.es (M. Fernández-Torrijos).

https://doi.org/10.1016/j.applthermaleng.2021.117801
Received 29 July 2021; Received in revised form 19 October 2021; Accepted 7 November 2021
Available online 26 November 2021

Turchi et al. [3] summarized the results of several studies contracted with WorleyParsons Group and results from their own SAM simulations to evaluate the impact of dry, wet and hybrid (both dry and wet operating in parallel) cooling systems on the performance and LCOE of parabolic trough CSP plants. They concluded that the transition from 100% wet to 100% dry cooling will result in LCOE increase of approximately 3% to 8% for parabolic trough plants throughout most of the southwestern United States locations while a water consumption reduction over 90%. Besides, they observed that hybrid cooling could reduce the LCOE increase, but this effect would be minimal for the Alamosa location, while clearly beneficial for Las Vegas location. The authors stated that the water cost, which was not varied in their calculations, has a major influence on the results and should be considered in future analysis. Another study developed later [4] where the effect of the time of delivery (TOD) rate factors (multiplying factor applied to the market purchase price of electricity at a given time of delivery period) was considered revealed that hybrid cooling can reduce the bid price of electricity when compared to exclusively dry cooled plants even in cooler climates like Alamosa, for heavily weighted TOD schedules.

Boukelia et al. [5] compared the effect of using dry cooling instead of wet cooling in a CSP plant of the power tower type in terms of thermodynamic yield (energetic and exergetic), and economic indicators (investment cost, net present value (NPV), and LCOE). The energy and economic analysis was performed using the mathematical model integrated within SAM software, and the location of the plant was Bechar, in South Algeria. They concluded that the annual power generation decreased more than 6.70% for the dry cooling compared to the wet cooling and the LCOE increased more that 9.19%. However the annual water consumption reduced by almost 94.40%. The authors indicate that in order to combine the advantages of dry and wet cooling systems, hybrid options should be explored.

Boulay et al. [6] developed a methodology to evaluate the impact of hybrid cooling system design on operating performance and economics of a coal-burning power plant comparing the increased revenue relative to the capital cost increment for different size dry cooling cases and a hybrid case at two different plant locations, taking into account the hourly ambient conditions and market energy prices. They concluded that unless there are revenue payments based on available summer capacity, the additional revenue for the increased energy produced by larger ACCs or hybrid systems are not sufficient to justify the increased capital cost when compared to the base case (dry system with the lowest capital cost). Concerning solar towers, Marugán-Cruz et al. [7] proposed the use of a dry Heller cooling system to diminish the water consumption of these CSP plants. In the system presented the water vapor from the turbine condenses in a direct contact jet condenser where it gets in contact with liquid water coming form a natural draft dry cooling tower. Then, part of the condensate returns to the cycle while the rest is pumped to the tower where it rejects the heat to the air. The study concludes that the annual energy production using the Heller system proposed is only 3.64% smaller compared to mechanical draft wet cooling system, while it is 5.97% greater compared to a ACC cooling system. For the location studied (Tonopah, Nevada USA), the total lifetime cost of the Heller cooling system could be smaller than the cost of the wet cooling system as long as the total costs of water are higher than 1.96 $/m^3. Rohani et al. [8] simulated a parabolic trough plant and a power tower plant to calculate the annual energy produced and water consumed by the different systems of the power plant (including solar field cleaning, steam cycle and cooling system). Besides two different water management plans are compared with the basic scenario (without water reuse) in terms of water consumption and LCOE, i.e. reusing the water of certain effluents or minimizing the blowdown in the cooling tower. The evaluation of theses alternatives was performed for different cooling systems: ACCs, steam surface condenser with the cooling water provided by a cooling tower and a hybrid system consisting of the combination of the former two.

In light of the research conducted on hybrid condensing systems for CSP plants there is a lack of thermo-economic studies of CSP plants of the tower type that allow to decide which type of system is most cost-effective (dry or hybrid) and which is the proportion of the cooling load that should be covered by the wet subsystem. The models developed with this aim should consider the water price since it is a key parameter in the economical performance of the plant. This paper investigates the effect of the type of cooling system (dry or hybrid) on the energy and economical performance of a solar tower plant. The results include the annual performance of a plant located at Dunhuang in Gansu, (China) and analyze the effect of the water price. No previous references have been found considering the effect of the water price on the economical performance of solar towers. The effect of the ambient conditions on the behavior of the dry (ACCs) and wet cooling systems (surface condenser cooled by a mechanical-draft cooling tower) are also evaluated.

2. Modeling

The CSP plant consists of 3 subsystems: the solar subsystem, the steam generators with the power block and the cooling subsystem. The solar field, the evaporation train and the power block are similar to those described in detail in Marugán-Cruz et al. [7]. The cooling system is either an air cooling system or a hybrid system that combines air cooled condensers and wet mechanically driven cooling towers. Fig. 1 shows the different subsystems of the CSP plant and the fluid flows.

2.1. Solar subsystem

The solar subsystem comprises the solar field, the solar receiver and the storage system. The solar field consists of thousands of heliostats or mirrors that follow the sun and concentrate the solar radiation on an external receiver located at the top of a tower. The receiver is a 360° tubular receiver formed by metal pipes, gathered into panels, that absorb the radiation and transfer it to the heat transfer fluid flowing through them. The fluid (molten salts) enters the receiver at 290 °C and exits at 565 °C and it is sent to the hot tank.

The solar field considered in this study is a radial staggered arrangement surrounding the receiver and north biased. The heliostat field has been generated with the software FluxSPT [9], representing a field similar to that of Crescent Dunes (Tonopah, Nevada). The field consists of 10,300 square mirrors of 10.5 m side.

To calculate the solar field efficiency SolarPILOT software [10] has been employed. The efficiency of the heliostats depends on, among others, the height of the receiver, the position of the mirrors, the aiming strategy, the day of the year and the solar time, and therefore, these values should be estimated at every hour. This software is able to determine the optical efficiency of each heliostat, the flux heat density and the concentration map or the ratio of flux density on the receiver at the top of the tower. To model the hourly performance of the solar plant the following assumptions have been made regarding the atmospheric conditions: a cloudless year with visual range of 40 km and limb-darkened sun model. The simulation model employed is a Hermite simulation with 25 × 25 grid resolution. A probability shift aiming method with a normal distribution strategy with a maximum allowable peak flux of 1500 kW/m^2 has been chosen to simulate the incident radiation on the receiver. To reduce the calculation time, Wagner [11] proposed to select at least 8 representative days to estimate the yearly flux distribution. These days are: 172, 218, 238, 256, 272, 290, 310 and 355. For each of those days the hourly average efficiency of each heliostat, $\eta_{hel,i}$, has been obtained.

Therefore, the incident heat power on the receiver, Q_{rec}, can been calculated as follows:

$$Q_{rec} = \sum_{i=1}^{n_{hel}} \eta_{hel,i}\, \rho\, \mathrm{DNI}\, A_{hel} \quad (1)$$

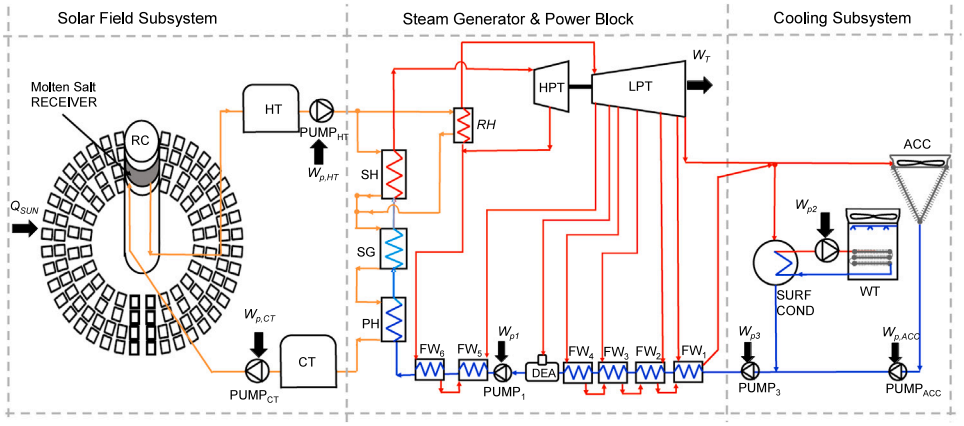

Fig. 1. Process flow diagram of the CSP plant with hybrid cooling system. Lines: Orange line: molten salts; blue line: liquid water; red line: steam. **R**: Receiver, **HT**: Hot salt storage tank, **CT**: Cold salt storage tank, **PH**: Preheater. **SG**: Steam generator, **SH**: Super-heater, **RH**: Reheater, **HPT**: High pressure turbine, **LPT**: Low pressure turbine, **FW**: Feedwater heater, **DEA**: Deaerator, **ACC** Air cooled condenser, **WT**: Wet tower.

Table 1
Geometrical parameters of the solar subsystem.

Parameter	Value
Optical tower height, H_{tower} (m)	180
Receiver height (m), H_{rec}	21.6
Receiver diameter (m), D_{rec}	17.6
Field boundary radius, (m)	1380
North shift of the boundary (m)	240
Number of heliostats, n_{hel}	10,300
Heliostat area, A_{hel} (m^2)	110.25
Solar field area, A_{SF} (ha)	676
Number of panels	16
Number of tubes per panel	76
Internal tube diameter (m)	0.042

where n_{hel} is the number of heliostats, $\rho = 0.95$ is the reflectivity of the mirrors, DNI is the hourly direct irradiation for a typical meteorological year obtained at PVGIS [12] and A_{hel} is the area of each heliostat. This incident heat power, Q_{rec}, is partly absorbed by the molten salts circulating through the tubes and partly lost by convection and radiation.

As the molten salt enters into the receiver it is divided into two flow paths, passing through half of the panels that form the receiver. In each panel the salt is divided into the 76 tubes that compose the panel, and, as long as the flow regime of the molten salts through the tubes is under the turbulent regime [13], the total mass flow rate through the receiver, $\dot{m}_{salt}$, can be calculated as:

$$\dot{m}_{salt} = \frac{Q_{salt}}{c_p\left(T_o - T_i\right)} \tag{2}$$

where $c_p = 1.52\,\mathrm{kJ/kg°C}$ is the specific heat [14] and $T_o = 565$ °C and $T_i = 290$ °C are the outlet and inlet temperature of the receiver, and Q_{salt} is the heat rate absorbed by the molten salts as they flow through the receiver that can be calculated as: $Q_{salt} = \eta_{rec}\, Q_{rec}$, where $\eta_{rec} = 0.8$ is the thermal efficiency of the receiver.

If the heat rate absorbed by the molten salts through the receiver, Q_{salt}, is higher than the mass flow rate needed to produce the steam to run the power block, Q_{in}, then the exceeding mass of the hot salts can be stored to be later used when there is no solar irradiation. Hence, electricity production can be decoupled from the solar resource. Similarly to Crescent Dunes solar tower plant, a two-tank molten salt storage system with a storage capacity of 10 h ($n_{st} = 10$ h) has been considered.

The main design parameters of the solar tower plant are described in Table 1.

Under nominal conditions the molten salts are able to produce a constant mass flow rate of steam of 87.46 kg/s at high temperature and pressure, which corresponds to full load conditions of the steam turbine. The heat supplied by the molten salts at the heat exchangers is $Q_{in} = 244.98$ MW.

2.2. Power block and steam generator

The hot molten salts enter the superheater and reheater at 565 °C and leave the preheater at 290 °C (see Fig. 1). Under nominal conditions the steam mass flow rate at the exit of the superheater (or the inlet of the high pressure turbine) is 87.46 kg/s at 550 °C and 126 bar, and the thermal efficiency of the power block is 44.1% while the mass flow rate of the steam through the condenser is $\dot{m}_c = 61.07$ kg/s.

The power block considered in this work is a reheated and regenerative Rankine cycle, with six closed feedwater heaters and a deaerator, commonly used in CSP plants (see Fig. 1). The details of the power block can be found in Marugán-Cruz et al. [7].

Due to the freezing (240 °C) and decomposition (565 °C) of the molten salts, the temperatures at the exit of the last feedwater heater (245 °C) and at the inlet of the high pressure turbine (550 °C) are limited. These temperature limitations reduce the efficiency of the power block. Moreover, the variation of the pressure at the outlet of the turbine affects the mass flow rate and the pressure at the extraction lines, and hence the net power, the efficiency of the power block and the heat rejected by the condenser change when the condensing pressure is not the nominal condensing pressure ($p_c = 0.1$ bar). The variation of the enthalpy at the end of the expansion line has been calculated using the method proposed by Spencer et al. [15],Srinivasan [16] and modified by Marugán-Cruz et al. [7], and the net power produced at the power block can be calculated as:

$$W_{PB} = W_{PB,ref} - \dot{m}_c\left(a\, p_c^b - \Delta h_{ref}\right) \tag{3}$$

where $W_{PB,ref}$ is the net power produced by the power block under design conditions, $a = 6.266\,10^5$ [J/kg Pa^{-b}], $b = 9.759 \cdot 10^{-2}$, $c = 1.441 \cdot 10^6$ [J/kg] and $\Delta h_{ref} = 9.84 \cdot 10^4$ [J/kg].

2.3. Condensing system

In this work, a comparison of the impact of dry versus hybrid condensing systems on energy and economical performance of solar tower plants was conducted. The dry condensing system consists of several air-cooled condenser cells connected in parallel, while the hybrid cooling consists of a parallel condensing system where the condensing steam is split between some air-cooled condensers, and a steam condenser where circulating water is cooled in one or more wet cooling towers connected in parallel. To analyze both dry and hybrid condensing systems, the air-cooled condenser and the system formed

Table 2
Heat transfer condensing system equations.

	Air-cooled condenser	Surface condenser	Wet cooling tower
Q	$\dot{m}_c(h_{c,i}-h_{c,o})=\dot{m}_a\,c_{p,a}(T_{a,o}-T_{a,i})$	$\dot{m}_c(h_{c,i}-h_{c,o})=\dot{m}_w\,c_{p,w}\,(T_{w,o}-T_{w,i})$	$\dot{m}_w\,c_{p,w}\,(T_{w,i}-T_{w,o})=\dot{m}_a\,(h_{a,o}-h_{a,i})$
Q_{max}	$\dot{m}_a\,c_{p,a}(T_c-T_{a,i})$	$\dot{m}_w\,c_{p,w}\,(T_c-T_{w,i})$	$CR_{min}\,\left(h_{sat,w,i}-\lambda-h_{a,i}\right)$
ε	$1-\exp(-NTU)$	$1-\exp(-NTU)$	$\dfrac{1-\exp\left[-NTU\,(1-C_e)\right]}{1-C_e\,\exp\left[-NTU\,(1-C_e)\right]}$
NTU	$\dfrac{UA}{\dot{m}_a\,c_{p,a}}$	$\dfrac{UA}{\dot{m}_w\,c_{p,w}}$	$\dfrac{Me\,\dot{m}_w}{CR_{min}}$
$UA,\ Me$	$\left[\dfrac{1}{h_{ae}A_a}+\dfrac{1}{h_cA_c}\right]^{-1}$	$\left[\dfrac{d_o}{d_i}R''_{tf}+\dfrac{1}{U_{cl}}\right]^{-1}\ n_t\,n_{wp}\,\pi\,d_o\,L_s$	$\dfrac{h_{drz}\,a_{rz}\,H_{Ti}}{G_w}+\dfrac{h_{dfi}\,a_{fi}\,L_{fi}}{G_w}+\dfrac{h_{dsp}\,a_{sp}\,L_{sp}}{G_w}$

Table 3
Draft equations of the condensing system.

Air-cooled condenser
$\Delta p_{Fs}=\dfrac{K_{ts}}{2\,\rho_i}\left(\dfrac{\dot{m}_a}{A_{fr}}\right)^2+\dfrac{K_{up}}{2\,\rho_o}\left(\dfrac{\dot{m}_a}{A_e}\right)^2+\dfrac{K_{do}}{2\,\rho_o}\left(\dfrac{\dot{m}_a}{A_e}\right)^2+\dfrac{K_{\theta t}}{2\,\rho_{io}}\left(\dfrac{\dot{m}_a}{A_{fr}}\right)^2+$
$p_a\left[\left(1-\dfrac{0.00975(0.5\,L_t\,\cos\theta+H_{dif})}{T_{a,o}}\right)^{3.5}-\left(1-\dfrac{0.00975(0.5\,L_t\,\cos\theta+H_{dif})}{T_a}\right)^{3.5}\right]$
$\Delta p_{Frs}=320.85-6.9604\,V_{Fr}+0.31373\,V_{Fr}^2-0.021393\,V_{Fr}^3$
$W_{Fr}=(4245.1-64.134\,V_{Fr}+17.586\,V_{Fr}^2-0.71079\,V_{Fr}^3)$
Surface condenser
$\Delta p_{Fs}=\left(\dfrac{L_s}{2\,d_i}\,f\,+1.25\right)n_{wp}\,\rho_w\left(\dfrac{V_F}{A_t\,n_t}\right)^2+\rho_w\,g\,H_{fi}$
$\Delta p_{Frs}=2\cdot10^5-1.65\cdot10^5\,V_{Fr}+2.46\cdot10^5\,V_{Fr}^2$
$W_{Fr}=V_F\,\dfrac{\left[\left(\frac{L_s}{2\,d_i}\,f\,+1.25\right)n_{wp}\,\rho_w\left(\frac{V_F}{A_t\,n_t}\right)^2+\rho_w\,g\,H_{fi}\right]}{4.1\,V_{Fr}-4.96\,V_{Fr}^2}$
Wet cooling tower
$\Delta p_{Fs}=\dfrac{\left(\sum K_i+K_{upfi}\right)}{2\,\rho_{av}}\left(\dfrac{\dot{m}_{av}}{A_{Tfr}}\right)^2$
$\Delta p_{Frs}=320.85-6.9604\,V_{Fr}+0.31373\,V_{Fr}^2-0.021393\,V_{Fr}^3$
$W_{Fr}=(4245.1-64.134\,V_{Fr}+17.586\,V_{Fr}^2-0.71079\,V_{Fr}^3)$

Table 4
Air-cooled condenser specifications and reference fan characteristics [17].

Parameter	Value
Hydraulic diameter d_e (m)	0.02975
Length of finned tube, L_t (m)	9.5
Number of tube rows, n_r (-)	2
Number of tubes per bundle (first row), $n_{tb(1)}$ (-)	57
Number of tubes per bundle (second row), $n_{tb(2)}$ (-)	58
Number of steam passes, n_{vp} (-)	1
Number of bundles, n_b (-)	8
Effective frontal area of one bundle (second row), A_{fr} (m^2)	27.55
Apex angle of V-frame, θ (°)	30
Fan diameter, d_F (m)	8
Fan hub diameter, d_h (m)	1.2
Test fan diameter, d_{Fr} (m)	1.536
Reference rotational speed, N_{Fr} (rpm)	750
Reference air density, ρ_r (kg/m^3)	1.2
Height of heat exchanger above ground level, H_{he} (m)	12
Diffuser height, H_{dif} (m)	3
Heat exchanger inlet support loss coefficient, K_{ts} (-)	1.5
Total loss coefficient for flow obstacles at the fan suction, K_{up} (-)	0.39
Total loss coefficient for flow obstacles at the fan discharge, K_{do} (-)	0.17

by the steam condenser and the wet cooling tower were modeled separately to obtain the condensing heat, parasitic consumption and water use for different operating parameters such as ambient temperature. The heat transfer and draft equations used in the modeling of both dry and hybrid condensing systems are summarize in Tables 2 and 3

2.3.1. Dry cooling system

The dry system proposed in this work consists of several air-cooled condenser units, or cells, connected in parallel. In this Section, the numerical model of an induced-draft air-cooled condenser formed by two rows of staggered, plate-finned, flattened tubes according to [17] is presented. The specifications of the air-cooled condenser can be seen in Table 4. For the air temperature (T_a), the atmospheric pressure (p_a) at the plant location, and given the fan rotational speed (N_F), the condensing temperature (T_c) and vapor quality at the outlet of the turbine (X), the energy and draft equations of the air-cooled condenser are solved to calculate the air mass flow rate ($\dot{m}_a$), air outlet temperature ($T_{a,o}$), fan shaft power (W_F) and condensate mass flow rate ($\dot{m}_c$). The energy equation to calculate the air outlet temperature is solved with an iterative procedure applying the Effectiveness-NTU method. Each row of the air-cooled condenser has different performance characteristics; thus the problem must be solved for each row separately. The outlet air temperature for each row is calculated from the effectiveness:

$$\varepsilon=\frac{Q}{Q_{max}} \tag{4}$$

where the effectiveness of a heat exchanger where a phase change occurs is calculated as shown in Table 2. Once the air outlet temperature of both first and second tube rows of the heat exchanger is obtained, the condensate flow rate out of the first and second tube rows are calculated from the energy balance assuming that all steam entering the tube is condensed.

To solve the energy equation to obtain the air outlet temperature, an initial value of the air mass flow rate ($\dot{m}_a$) is assumed for the iterative process. To confirm the value assumed for the air mass flow rate, the draft equation is solved (see Table 3). The heat exchanger inlet support loss coefficient K_{ts} and the total loss coefficients for flow obstacles at the fan suction K_{up} and discharge K_{do} are shown in Table 4. $K_{\theta t}$ is the total loss coefficient for the bundle with inlet and downstream losses due to oblique flow, which can be calculated with expression given in [17]. The actual fan static pressure difference Δp_{Fs} is related to the fan static pressure difference Δp_{Frs} (see Table 3) of a reference fan (reference values included in Table 4) by the fan affinity laws. Once the actual air volume flow rate through the fan (V_F) is obtained from the draft equation, the fan shaft power is obtained by the fan affinity laws from the reference fan power (see Table 3) given in [17]

2.3.2. Wet cooling system

The hybrid cooling system consists of a parallel condensing system where the condensing steam is split between several air-cooled condensers connected in parallel (dry cooling system), and a steam condenser where circulating water is cooled in one or more wet cooling towers connected in parallel (wet cooling system). To analyze the wet cooling system, the steam condenser is first studied to obtain some parameters such as the cooling water mass flow rate and outlet temperature that are inlet parameters for the wet cooling tower model (see Fig. 3).

Steam surface condenser

A tubular heat exchanger was modeled as the steam surface condenser for the cooling tower system. The specifications of the surface condenser can be seen in Table 5. Given the cooling water inlet temperature to the steam condenser ($T_{w,i}$), the pump rotational speed (N_F), the condensing temperature (T_c) and vapor quality at the outlet

Table 5
Steam surface condenser specifications. Reference conditions obtained from [17].

Parameter	Value
Tube external diameter d_o (mm)	28
Tube wall thickness, th (mm)	0.8
Length of tubes, L_s (m)	7.4
Number of cooling water passes, n_{wp} (-)	2
Number of tubes per pass and tower, n_t (-)	503
Reference cooling water density ρ_r (kg/m^3)	995.73
Reference rotational speed N_{Fr} (r.p.m.)	3000
Cooling water pressure p_w (atm)	5

Table 6
Cooling tower specifications and reference fan characteristics [17].

Parameter	Value
Tower height, H_T (m)	12.5
Fan height, H_F (m)	9.5
Tower inlet height, H_{Ti} (m)	4
Tower inlet width, W_{Ti} (m)	12
Tower breadth, B_{Ti} (m)	12
Fill height, L_{fi} (m)	1.878
Height of spray zone, L_{sp} (m)	0.5
Frontal area of the fill, A_{Tfr} (m^2)	$B_{Ti} \times W_{Ti}$
Fan diameter, d_F (m)	8
Reference fan diameter, d_{Fr} (m)	1.536
Reference fan rotational speed N_{Fr} (rpm)	750
Reference air density, ρ_r (kg/m^3)	1.2

of the turbine (X), the energy and draft equations of the surface condenser are solved to calculate the cooling water mass flow rate ($\dot{m}_w$), cooling water outlet temperature ($T_{w,o}$) and pump shaft power (W_P). The draft equation to calculate the cooling water mass flow rate is solved with an iterative procedure assuming that the cooling water outlet temperature is known. Water pressure drop along the surface condenser tubes is calculated as shown in Table 3, where f is the friction factor obtained from a formulation by Bhatti and Shah for hydraulically smooth tubes [18]

$$f = 0.00512 + 0.4572\, Re_w^{-0.311} \tag{5}$$

where $Re_w = V_F\, d_i\, \rho_w/(\mu_w\, A_t\, n_t)$.

The actual pump static pressure difference Δp_{Fs} is related to the pump static pressure difference Δp_{Frs} (see Table 3) of a reference pump (see reference conditions in Table 5) by the affinity laws. Thus, the cooling water volume flow rate V_F is obtained solving the draft equation and the pump power consumption is calculated as a function of the water pressure drop along the surface condenser tubes and the pump efficiency (see Table 3). Once the cooling water volume flow rate V_F is calculated from the draft equation, the Effectiveness-NTU method (see Table 2) is applied to confirm the value assumed for the cooling water outlet temperature. The calculation of the overall heat transfer coefficient of clean condenser U_{cl} is based on the HEI Standards of Steam Surface Condensers [19]

$$U_{cl} = 2.7 \left(\frac{V_F}{A_t\, n_t}\right)^2 F_m\,(0.5707 + 0.0274\, T_{w,i} - 0.00036\, T_{w,i}^2) \tag{6}$$

where $F_m = 0.87$ for stainless steel tubes [20]. The overall heat transfer coefficient for the surface condenser considers also the tube fouling by means of a tube inside fouling resistance $R''_{tf} = 0.5 \cdot 10^{-5}$ [20].

Wet cooling tower

An induced-draft wet-cooling tower was modeled according to [17]. The specifications of the cooling tower can be seen in Table 6.

For the air temperature T_a, wet bulb temperature T_{wb} and atmospheric pressure (p_a) at the plant location and given the inlet water temperature ($T_{w,i}$), water outlet temperature ($T_{w,o}$) and water mass flow rate ($\dot{m}_w$) required by the steam surface condenser, the energy and draft equations of the cooling tower are solved to calculate the dry air mass flow rate ($\dot{m}_a$), air outlet temperature ($T_{a,o}$), outlet pressure ($p_{a,o}$), fan rotational speed (N_F), fan shaft power (W_F) and rate of water evaporation ($\dot{m}_{ev}$). The energy equation to calculate the air outlet temperature is solved with an iterative procedure applying the Effectiveness-NTU method for evaporative systems [21], assuming that the air is saturated at the tower outlet. With this method the saturated air temperature at the tower outlet is determined from the effectiveness of the cooling tower. The Merkel transfer characteristic of the cooling tower, Me, (see Table 2) has been calculated taken the equations for the rain zone rz, the fill fi and the spray zone sp given in [17].

Once the temperature of the saturated air at the tower outlet has been obtained from the Effectiveness-NTU method, the mass flow rate $\dot{m}_a$ is calculated from the energy balance, and the amount of water lost due to evaporation can be calculated by:

$$\dot{m}_{w,ev} = \dot{m}_a\,(w_o - w_i) \tag{7}$$

Since a portion of the circulating water must be discharge as blowdown to keep the ratio of dissolved solids in the circulating water to that of the makeup water (cycle of concentration, N_c) below a reasonable value, and considering negligible drift losses, the total makeup water can be calculated from the evaporated water as

$$\dot{m}_{w,makeup} = \dot{m}_{w,ev}\left(\frac{N_c}{N_c - 1}\right) \tag{8}$$

where N_c has been taken equal to 3.

Besides, it is possible to confirm the value assumed for the pressure at the outlet of the fill (before the fan inlet) in the iterative procedure:

$$p_{a,o} = p_a \left[1 - \frac{0.00975\,(H_{Ti} + L_{fi}/2)}{T_a}\right]^{3.5(1+w_i)\left(1-\frac{w_i}{w_i+0.622}\right)} - \sum K_i \frac{(\dot{m}_{av}/A_{Tfr})^2}{(2\,\rho_{av})} \tag{9}$$

where $\dot{m}_{av}$ is the average air-vapor mass flow rate, ρ_{av} is the harmonic mean air-vapor density and the geometry parameters can be found in Table 6.

The loss coefficients K_i of the different tower elements can be calculated with correlations and performance data provided in [17].

On the other hand, the draft equation of the cooling tower is solved to calculate the rotational speed of the fan N_F (see Table 3), where the fan upstream loss coefficient K_{upfi} can be calculated with the expression given in [17] and the static pressure difference Δp_{Fs} and the actual flow rate of the fan V_F are related to the fan static pressure difference Δp_{Frs} (see Table 3) and the flow rate of a reference fan respectively (reference values included in Table 6) by the fan affinity laws. Once the actual rotational speed of the fan (N_F) is obtained from the draft equation, the fan shaft power is obtained by the fan affinity laws from the reference fan power (see Table 3) given in [17].

2.3.3. Operating restrictions

In this section, inequality constraints are written to define the feasible region for the optimization problem, as well as feasible operating conditions for an optimal air-cooled condenser, surface condenser and cooling tower. First of all, condensing temperature must be the maximum temperature of the cooling system. The effectiveness of all the heat exchangers is lower than 100%; thus, the air outlet temperature in the air-cooled condenser must be lower than the steam condensing temperature, the cooling water outlet temperature to the surface condenser $T_{w,o,SC}$, must be lower than the steam condensing temperature, and the cooling water outlet temperature from the cooling tower $T_{w,o,WT}$ must be higher than the wet-bulb air temperature. Moreover, an upper limit of 50 °C on the cooling water inlet temperature $T_{w,i,WT}$ is specified to avoid fouling, scaling and corrosion [22], and the water-to-air mass flow ratio in the cooling tower must be in the range $0.5 < \dot{m}_w/\dot{m}_a < 2.5$ according to Singham [23]. Feasibility constraints are summarized in Fig. 2 for the different elements of the cooling elements.

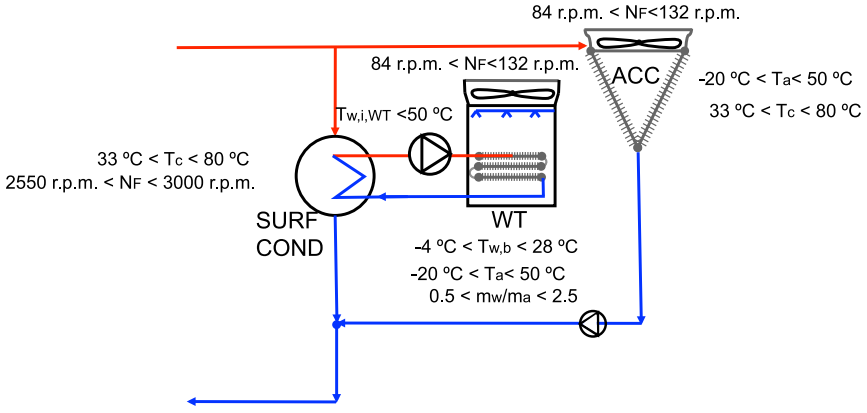

Fig. 2. Cooling system feasibility constraints.

2.4. Solution procedure

The main purpose of this work is to optimize the cooling system operation parameters to maximize the power plant revenue. Two different cooling systems have been analyzed: a dry cooling system formed by several air-cooled condenser units n_{ACC} connected in parallel, and hybrid cooling system where the condensing steam is split between the air-cooled condenser system and a steam condenser which circulating water is cooled in one or more wet cooling towers n_{WT} (see Fig. 1). Thus, the total heat rated dissipated by the cooling system is obtained as:

$$Q_c = n_{ACC}\, Q_{ACC} + n_{WT}\, Q_{WT} \tag{10}$$

where Q_{ACC} is the heating load rejected by a single unit of air-cooled condenser, and Q_{WT} is the heating load dissipated by a single unit of cooling tower.

To calculate the heat rate rejected by a single unit of both air-cooled condenser and wet cooling tower, independent simulations of each cooling subsystem were conducted varying different inlet parameters. For the simulations of the dry cooling system, the dry-air temperature was varied from −20 to 50 °C and the fan rotational speed was varied from 84 to 132 r.p.m. For the simulations of the wet cooling system, the wet-bulb air temperature was varied from −4 to 28 °C, the cooling water inlet temperature to the surface condenser was varied from 10 to 40 °C, the pump rotational speed was varied from 2250 to 3000 r.p.m., and the wet cooling tower fan rotational speed was varied from 84 to 132 r.p.m. In both dry and wet cooling systems, the condensing temperature was varied from 33 to 80 °C (see Fig. 2).

The cooling system analyzed in this work is part of the solar thermal Rankine power plant proposed by Marugán-Cruz et al. [7]. Comparing the cooling load required by the Rankine cycle with the heat rate dissipated by the cooling system (Eq. (10)) obtained from the simulations of each cooling subsystem separately, different combinations of the operation parameters such as the number of both air-cooled condensers and wet cooling towers working, the condensing temperature, the fan and pump rotational speeds, and the cooling water temperature might be possible for each ambient conditions. The best combination of parameters is the one that maximizes the revenue, which is calculated as the difference between the earning due to the net energy produced by the power plant, E_{net}, and the total makeup water costs. Therefore the revenues can be calculated as:

$$B = P_e\, E_{net} - P_w\, \frac{n_{WT}\, m_{w,makeup}}{\rho} \tag{11}$$

where B is the hourly revenue, P_e is the electricity price, P_w is the water price. Notice that the hourly net energy, E_{net}, is the energy produced by the power block, minus the parasitic consumption due to the air-cooled and cooling tower fans, the steam condenser and air-cooled pumps (see Eq. (12))

$$E_{net} = E_{PB} - n_{WT}\,(E_{F,WT} + E_{P,WT}) - n_{ACC}(E_{F,ACC} + E_{P,ACC}) \tag{12}$$

$E_{F,WT}$ is the hourly energy consumed by the wet cooling tower fan, $E_{P,WT}$ is the hourly energy consumed by the wet cooling tower pump, $E_{F,ACC}$ is the hourly energy consumed by the air-cooled fan, $m_{w,makeup}$ is the hourly makeup water, and $E_{P,ACC}$ is the hourly energy consumed by the downstream air-cooled condenser pump, which is necessary to rise the air-cooled condenser outlet pressure to the saturation pressure p_c. Note that the condensation process does not take place at a constant steam temperature in the air-cooled condenser due to the pressure changes along the finned tubes, whereas the pressure drop of the condensing water along the surface condenser is negligible compared to the pressure drop of the condensing water along the air-cooled condenser. Thus, in sake of simplicity, the condensation process is considered to take place at a constant steam temperature and pressure in the surface condenser, whereas the pressure and temperature drops along the air-cooled condenser were considered in the calculations. As both condensing water streams from the surface condenser and from the air-cooled condenser are mixed before being pumped by PUMP 3 to the feedwater heaters, an additional pump (P, ACC) downstream the air-cooled condenser is necessary to rise the air-cooled condenser outlet pressure to the saturation pressure p_c (see Fig. 1). The hourly energy required by the air-cooled condenser pump is calculated as

$$E_{P,ACC} = m_c\,(h_{sat}(T_c) - h_{c,o}) \tag{13}$$

where m_c is the hourly water mass-flow through the air-cooled tube-bundles, $h_{c,o}$ is the specific enthalpy of the condensing steam at the outlet of the air-cooled condenser, and $h_{sat}(T_c)$ is the saturated water specific enthalpy evaluated at the condensing temperature T_c.

Fig. 3 shows the calculation algorithm used in this work to accomplish the cooling system optimization and analyze the anual operation of a solar tower power plant.

3. Results

3.1. Simulation of the cooling system with variable inlet parameters

The cooling system proposed in this work consists of a combination of two systems connected in parallel: (i) air-cooled condensers (see Section 2.3.1); (ii) steam surface condenser with cooling towers (see Section 2.3.2). Independent simulations of each system were conducted varying different inlet parameters to obtain the dissipated heat and net energy produced. The inlet parameters for the air-cooled condenser system were the dry-air temperature, the condensing temperature, and the fan rotational speed. Fig. 4 shows the results of heat dissipated by the air-cooled condenser and fan power consumption as a function of

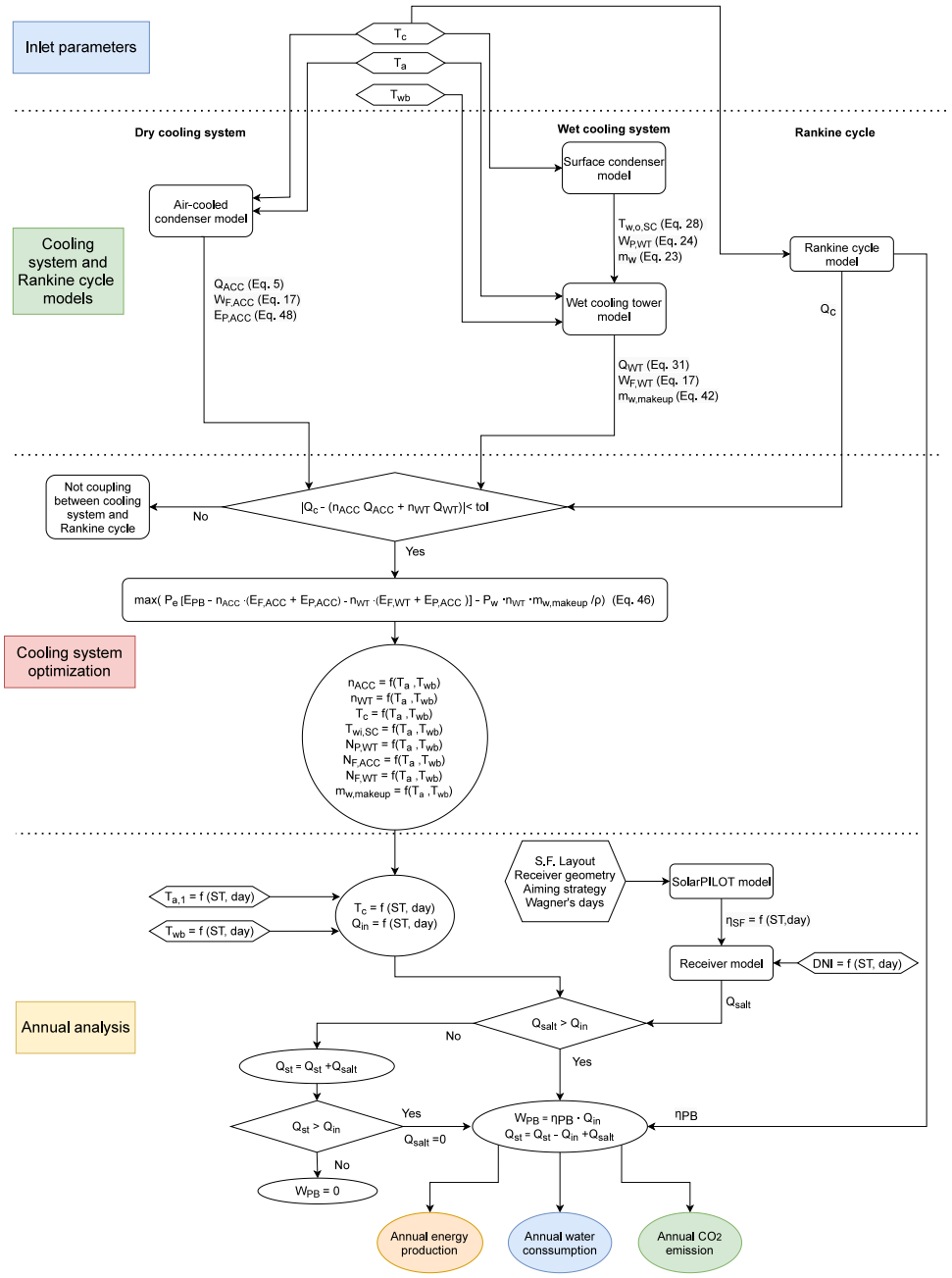

Fig. 3. Calculation algorithm.

the dry-air and condensing temperatures, for different fan rotational speeds. As shown, keeping constant the dry-air temperature, higher condensing temperatures result in higher heating load at the condenser and, therefore, lower efficiency. Besides, the energy consumed by the fan has a strong dependence on the rotational speed, but it is almost independent from the condensing and dry-air temperatures.

The variable inlet parameters for the system formed by the steam surface condenser and the cooling tower were the dry-bulb and wet-bulb temperatures, the condensing temperature, the surface condenser pump rotational speed, and the cooling water inlet temperature to the surface condenser (which is the outlet temperature of the cooling tower). Fig. 5 shows the results of the power released by the cooling tower system and the fan power consumption as a function of the wet-bulb and condensing temperatures, for different cooling water inlet temperature to the steam surface, for a pump rotational speed of 2550 r.p.m. As shown, most of the wet-bulb and condensing temperature combinations give results that do not satisfy the cooling tower operation constraints (see Fig. 2). Fig. 5 shows that the wet-bulb temperature has a strong influence on the water outlet temperature, as the former must be lower than the latter. Comparing Figs. 5 and 6, it is shown that higher rotational speeds of the surface condenser pump result in higher temperature differences between the outlet cooling water temperature and the wet-bulb air temperature, which results in lower condensing temperatures for a given wet-bulb temperature. However, as the cooling water mass flow rate increases with the surface condenser pump rotational speed, the air mass flow rate circulating through the cooling tower and then, the fan power consumption also increases.

Comparing the condensing temperature results for dry and wet cooling systems (Figs. 4–6), the maximum condensing temperature is reduced from 80 °C for the air-cooled condenser system to 60 °C for the wet cooling system (a valid solution that satisfies the wet cooling

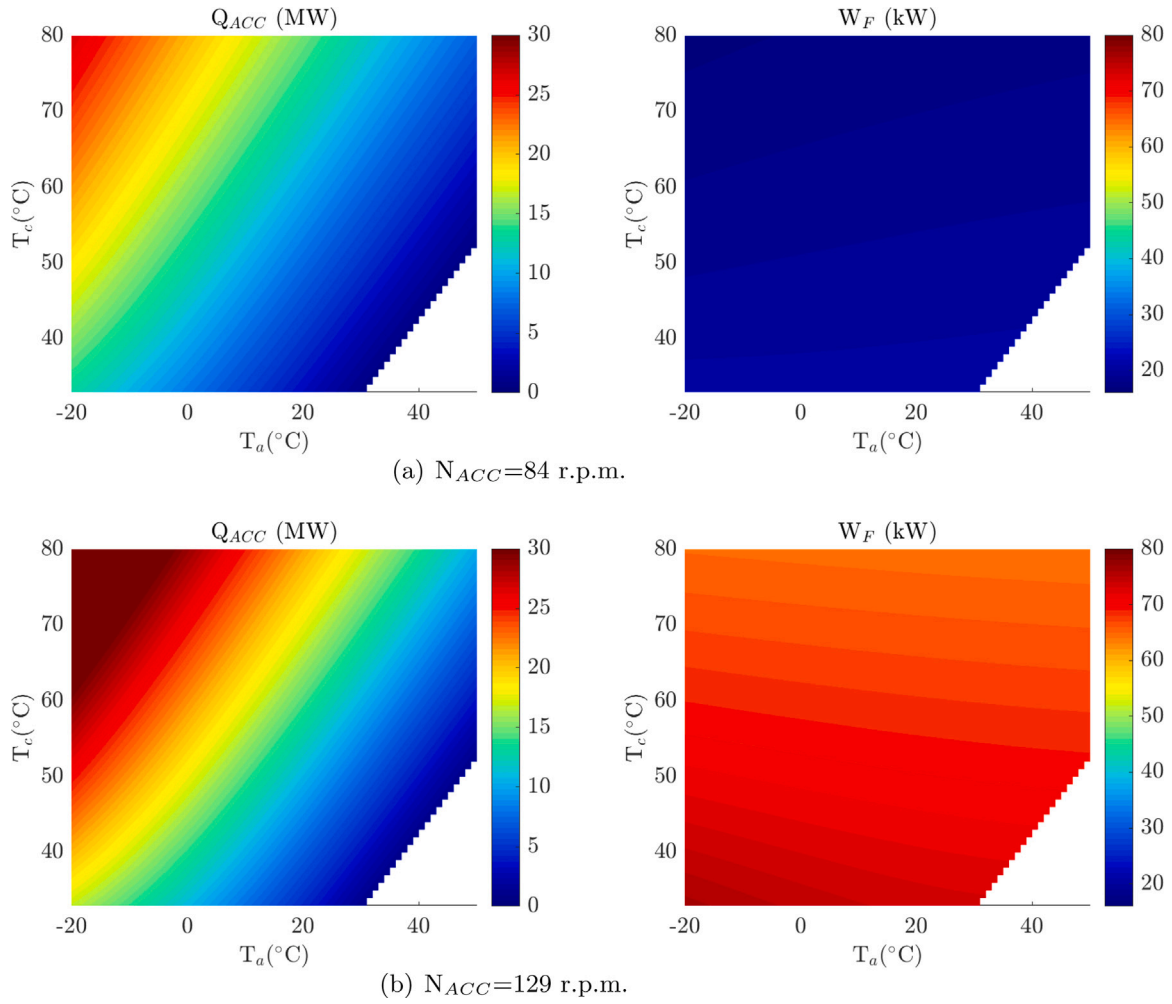

Fig. 4. Air-cooled condenser heat transfer rate and fan power consumption for different fan rotational speeds.

tower operation constraints was not found for condensing temperatures higher than 60 °C).

3.2. Optimization of the cooling system inlet parameters

Once the numerical simulations of each cooling subsystem was conducted varying different inlet parameters, an optimization process was carried out to determine the inlet parameters (i.e. the number of working ACC and wet tower units, the condensing temperature) that maximize the power plant revenues obtained after subtracting the water cost. The results of the optimization depend on the ratio of the water to electricity prices, $R = P_w/P_e$, where P_w is the water price ($/m^3) and P_e is the electricity price ($/kWh$_e$): low water to electricity prices will lead to a higher use of the wet tower units and therefore a higher efficiency of the power plant while high water to electricity prices will lead to a reduction of the use of the wet cooling towers, higher condensing temperatures and a reduction of the efficiency of the CSP plant.

The left column of Fig. 7 shows the condensation temperature and the net power supplied by the CSP plant as a function of the ambient temperature, whereas the right column shows the average number of working ACC and wet tower units at each ambient temperature, for the different condenser systems studied: dry system with 16, 20 or 24 ACCs connected in parallel, and hybrid system where the condensing steam is split between 16, 20 or 24 ACCs and a steam condenser which circulating water is cooled in 1, 2 or 3 wet towers. The operation strategy of the cooling system is to increase the number of working ACCs and wet towers as the ambient temperature increases. As a cooling system operation condition, the wet towers are not operating for dry-bulb temperatures below 0 °C, and the ACC units are started-up in groups of four.

As expected for all the systems, the condensing temperature increases with the ambient temperature. However, at some points, the condensing temperature abruptly decreases, which is due to the start-up of a group of four ACC units. Comparing the cooling system with 1, 2 or 3 wet towers, it is shown that increasing the number of available wet towers reduces the condensing temperature of the system, which results in an increase of the efficiency of the power block and a rise of the net power supplied by the CSP plant. Comparing the net power supplied by the CSP for the cooling system with 16, 20 or 24 ACCs, it is shown that the higher the number of ACC available units, the higher the net power supply by the CSP for a certain ambient temperature.

3.3. Solar tower plant annual analysis

Once the optimization process was conducted to determine the cooling system operation parameters for each dry and wet-bulb air temperatures, the annual operation of the CSP plant located in Dunhuang, China (40.03° N, 94.25° E) was analyzed comparing the effect of having a dry or hybrid cooling system. Dunhuang has an arid cold climate with very low precipitation and dry ambient temperature that ranges during the year from −17 °C to 37.4 °C (see Fig. 8(b)): it is very cold in winter with an average dry temperature of −2.6 °C that never exceeds 25 °C, while during the central days of the year (from the 10th of June

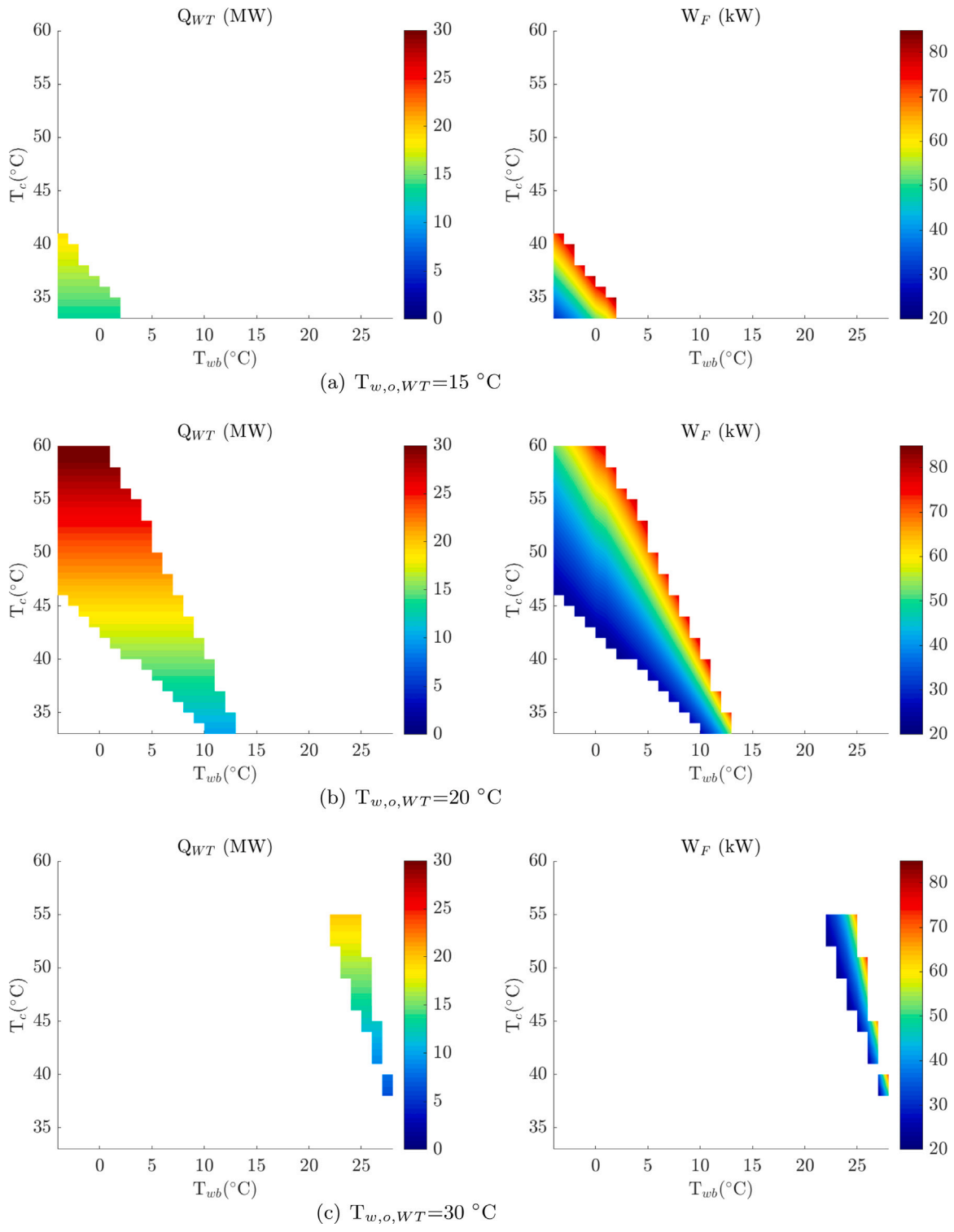

Fig. 5. Cooling tower heat transfer rate and fan power consumption for different cooling tower water outlet temperatures for surface condenser pump rotational speed of 2550 r.p.m.

to the 1st of September) the mean dry ambient temperature is 26.6 °C and it never falls under 15 °C. It has an average relative humidity of 23.7%, and the wet bulb temperature varies from −18.18 °C to 17.02 °C (see Fig. 8(c)). Based on the data of TMY [12], the solar annual direct normal irradiation in Dunhuang is 1923 kWh/m^2/year. The Köppen–Geiger system classifies the climate into five main classes, named A, B, C, D and E, the classes are divided into 6 sub-classes, and there are subgroups within the sub-classes depending on the temperature. According to the Köppen–Geiger climate system classification the solar tower plant of Dunhuang is located in a BWk climatic region (B: arid, W: desert, k: Cold) [24].

The performance of the CSP with the different cooling systems has been simulated and compared. The cooling systems here studied are: (i) dry cooling system with either 16, 20 or 24 ACC condensers; (ii) hybrid system composed of 16, 20 or 24 ACC condensers and 1, 2 or 3 wet towers. Independently of the condensation system, the total

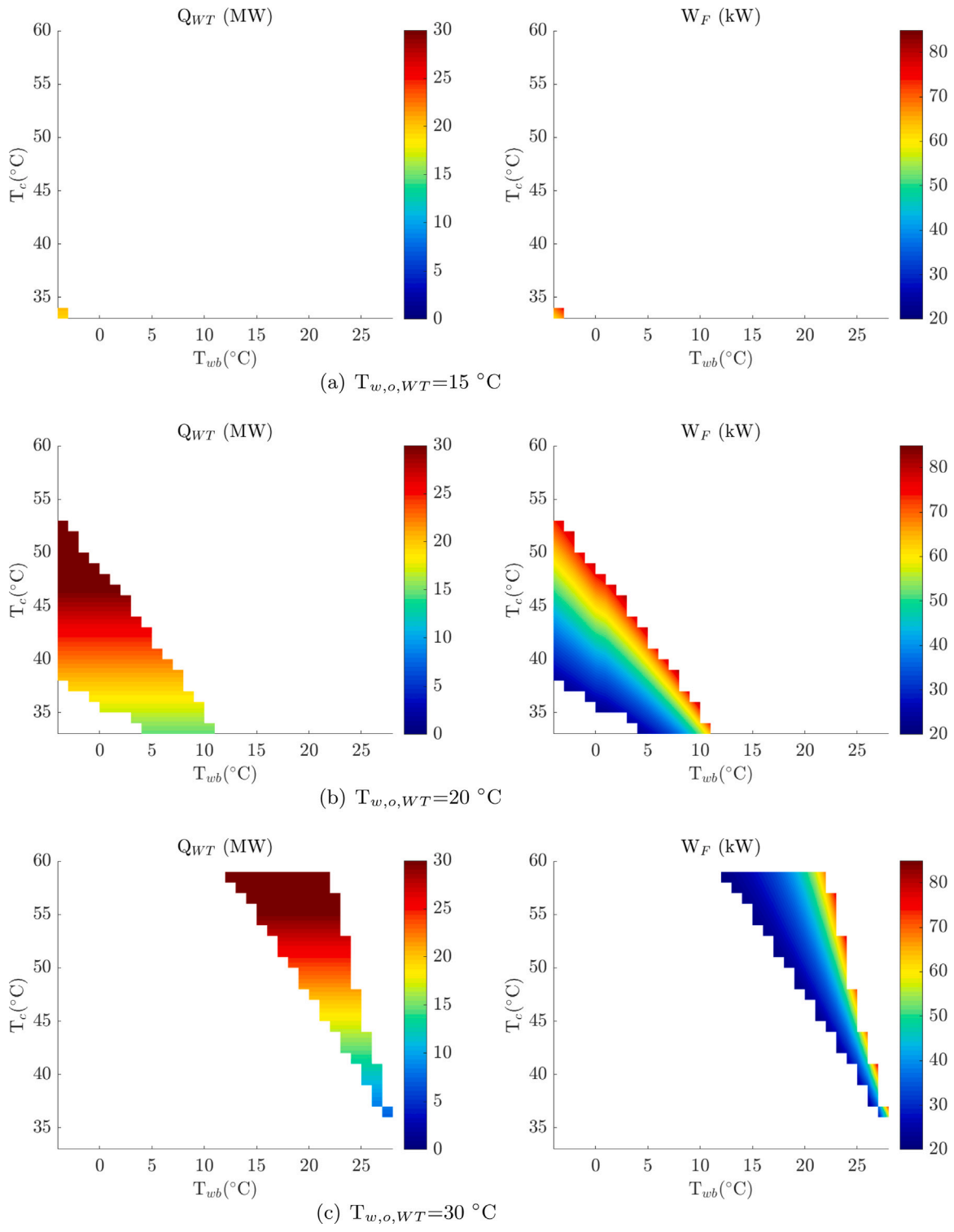

Fig. 6. Cooling tower heat transfer rate and fan power consumption for different cooling tower water outlet temperatures for surface condenser pump rotational speed of 3000 r.p.m.

number of working hours of the solar plant in Dunhuang is 5066 per year. Changing the condensing system varies the power output, since the condensing temperature varies, but the number of working hours remains the same, since the steam mass flow rate at the turbine inlet remains constant (see Section 2.2).

To select the optimum configuration of air-cooled condensers the operation of the plant has been analyzed for 16, 20 and 24 ACCs.

Fig. 9 shows a histogram of the number of hours with a given condensing temperature for the 3 dry configurations (16 (red), 20 (blue) and 24 ACC (green)) for the 10 h storage CSP plant in Dunhuang. It can be seen that the condensing temperature ranges from 33 C to 64 °C, depending on the condensing system. Furthermore, for the smallest condenser system (16 ACC) the condensing temperature reaches a temperature of 64 °C, while for the cases of 20 and 24 ACC

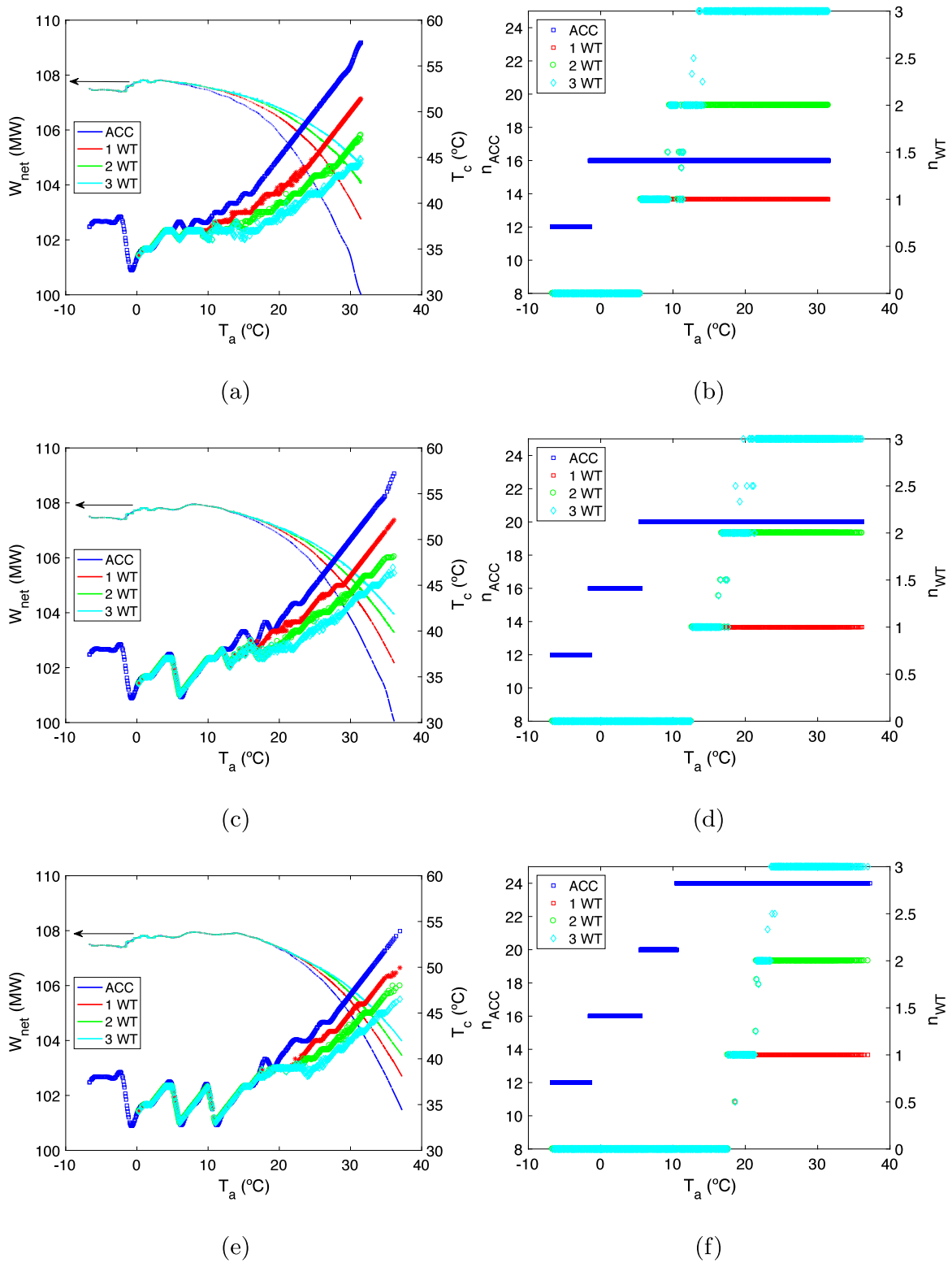

Fig. 7. Performance comparison with different condensing systems as a function of dry ambient temperature for the water to electricity price ratio of 10 ($/m^3)/($/kWh$_e$). Blue line corresponds to dry condensing system, whereas red, green and cyan lines correspond to hybrid systems with 1, 2 or 3 available wet cooling towers, respectively. (a),(c) and (e) Net power output (left axis) and condensing temperature (right axis) for 16, 20 and 24 ACC available cells respectively. (b), (d) and (f) Average number of working cells (left axis) of ACC dry condensing system and average number of wet cooling towers working (right axis) for 16, 20 and 24 ACC available cells respectively.

the maximum condensing temperature is of 58 °C and 54 °C respectively. Increasing the number of air condenser implies the condensation temperature decreases, and hence the number of hours that the cycle can operate at lower condensing temperatures. In particular, for the largest cooling system (24 ACC), 4033 h the condensing temperature is lower than the $T_{c,ref}$ = 45°C (that is close to 80% of the working hours), while for the 20 ACC system the number of hours working under the reference condensing temperature is 3607, (slightly bigger than 70% of the working hours), and for the 16 ACC system the fraction of time

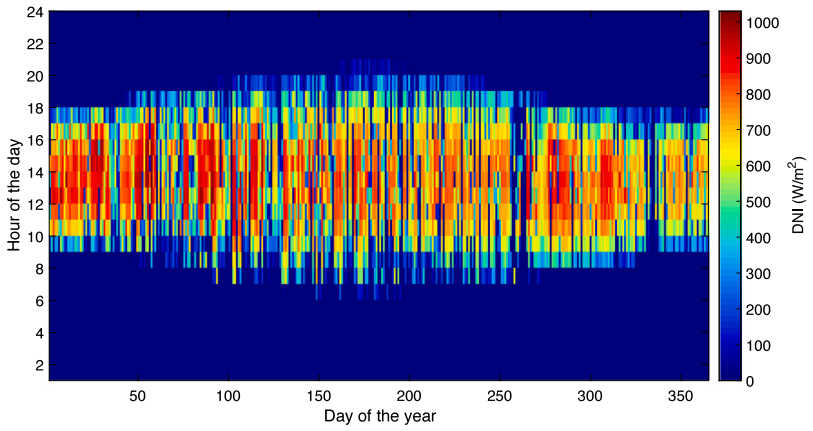

(a)

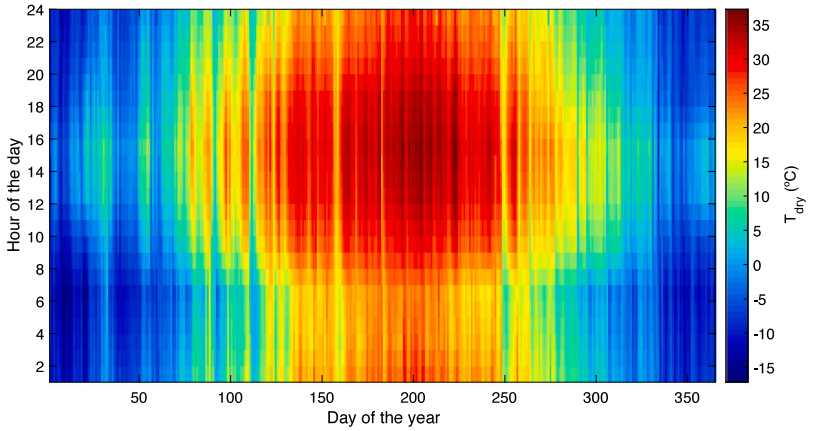

(b)

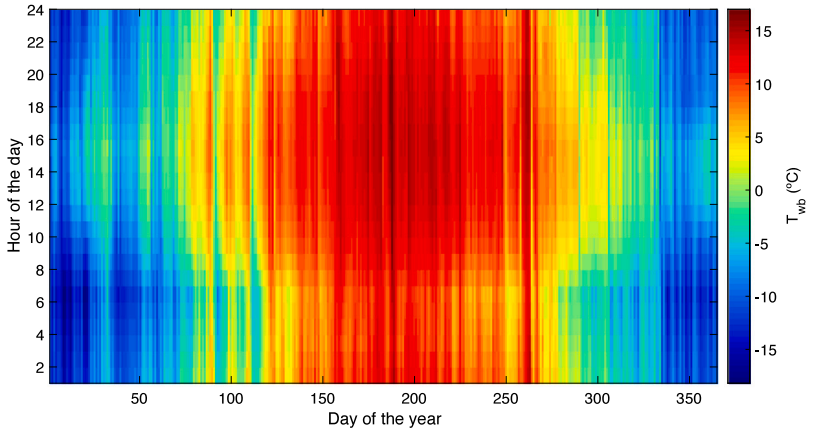

(c)

Fig. 8. Distribution of (a) DNI, (b) dry-bulb temperature and (c) wet bulb temperature, based on the data from Dunhuang (Gansu Sheng, China)[12].

that the condensing temperature is over the reference value is close to a 60% (or 2922 h).

Fig. 10 shows the number of working hours of the cooling towers for the 3 hybrid configurations (16 (top figure), 20 (middle figure) and 24 (bottom figure) ACC available cells). The blue bars show the number of hours where the steam is condensed only by the ACCs, red bars represent the hours when ACCs work in parallel with only one wet tower, green bars when ACCs work in parallel with two towers and cyan when three wet cooling towers are used to condense the steam in parallel with the ACC system. For the different configurations (16, 20 and 24 ACCs) as the ratio of the price of the water to electricity, R, increases the number of working hours of the wet cooling towers diminishes, becoming zero when this for a ratio R of 50 ($/m^3)/($/kWh$_e$). As the number of ACC cells increases the decay in the number of working hours of the wet cooling towers is faster because the heat condensed by the wet cooling system can be enhanced by increasing the number of cells working or by increasing the speed of the fans.

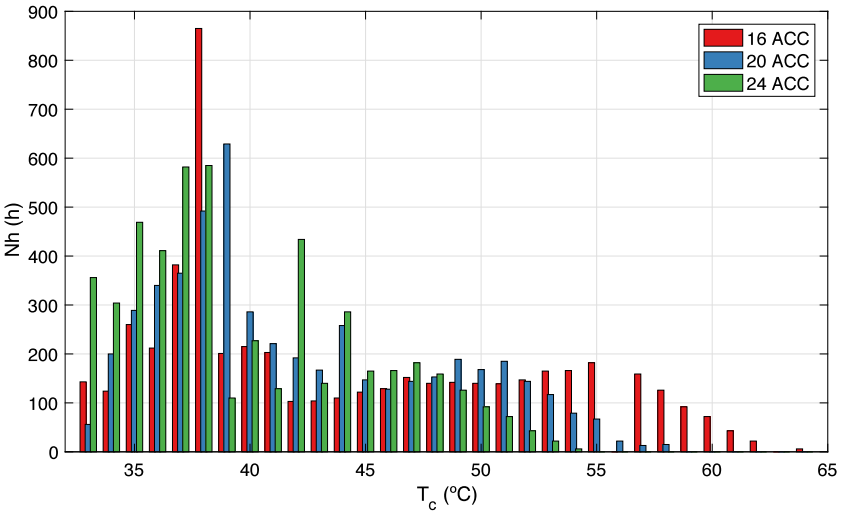

Fig. 9. Histogram of the condensation temperature for the different dry systems 16 ACC (red), 20 ACC (blue) and 24 ACC (green).

The condensing pressure (or temperature) and the heat transfer rate at the condenser depend on the cooling system and on ambient conditions: for dry cooling systems they depend on air dry bulb temperature and if the condensing system is a wet or hybrid cooling system they depend on wet bulb temperature too. Fig. 11 shows the annual distribution of the heat dissipated by the cooling system for the three different dry condensing systems with 16, 20 and 24 cells. It can be observed that the system is not working at certain hours of the day since the capacity of the storage system is not big enough to maintain the power block working the entire day. In addition, it can be seen that for cold days all three systems are able to reject the same heat rate, because the condensing temperature and hence the cycle efficiency is almost the same in the three cases, however as the dry ambient temperature increases the smaller the ACC system rejects the most heat. This is so because the 16 ACCs system is unable to reduce the condensing temperature as much as the other two, and therefore the cycle needs to reject more heat, and its efficiency is reduced. Note that when the condensation temperature varies, the mass flow rate of steam that goes to the condensation system $\dot{m}_c$ changes, since the mass flow rates at the different extraction lines also vary.

Fig. 12 shows the heat rejected by the different hybrid condensers for a water-to-electricity price of 10. The left column of Fig. 12 shows the distribution along the year of the heat rejected by the ACC units for hybrid cooling systems that have, either one, two or three wet cooling towers, whereas the right column shows the distribution of the heat rejected by the wet cooling tower units, for $R = 10$ ($/m^3)/($/kWh$_e$). As shown in the figure, when both dry and wet-bulb air temperatures increase (summer) a greater use of the cooling towers is needed to reduce the condensing temperature and therefore, to increase the power cycle efficiency, whereas during approximately 30% of the year (winter) the wet cooling towers are switched off. As expected, as the number of available wet tower units increases, the heat load rejected by the ACCs decreases, because a higher fraction of the condensation heat is dissipated in the wet part of the system. In fact, the wet cooling system goes from giving up to 20% (see Fig. 12 a and b) of the required power when only 1 wet tower is available, to give up to 50% when 3 wet towers are available (see Fig. 12 e and f).

3.4. Thermo-economic optimization

Based on the annual energy analysis using the TMY data of Dunhuang an economical comparison of the different condensing configurations has been performed using the Levelized Cost of Energy, $LCOE$ (c$/kWh$_e$). The LCOE is an economic indicator that measures the total costs over the energy yield, E_{ann} [25]. For a project with a constant energy output, constant operation and maintenance (O&M) costs, and no financing, the LCOE can be calculated as follows:

$$LCOE = \frac{C_{invest} \cdot (f_{ins,ann} + f_{cr}) + C_{OM}}{E_{ann}} \tag{14}$$

where C_{invest} are the investment costs, C_{OM} the O&M costs, f_{ins} the insurance costs and f_{cr} is the capital recovery factor, that depends on the discount rate i_r and the expected lifetime, n_{yr}, in years.

$$f_{cr} = \frac{i_r(1+i_r)^{n_{yr}}}{(1+i_r)^{n_{yr}} - 1} \tag{15}$$

Furthermore, the investment costs of a solar tower plant include the particular equipment of these plants, C_{solar} (solar field, solar mirrors, tower and receiver, thermal storage system and auxiliary systems), the conventional plant components and systems, C_{pp} (turbine, feed water heaters, grid connection), and the cooling system, C_{cool} (see Eq. (16)). It should be noticed that these costs comprehend contingency, f_{cont}, and indirect costs too, f_{ind}. Estimating these costs is complicated since the equipment and operation costs vary depending on the country and level of maturity of the technology and they are rarely published. In Table 7 the key parameters that affect the project costs are shown.

The investment costs of these plants can be calculated as follows:

$$C_{invest} = (C_{solar} + C_{pp} + C_{cool})(1 + f_{cont})(1 + f_{ind}) \tag{16}$$

where

$$C_{cool} = n_{ACC} \cdot C_{ACC} + n_{WT} \cdot C_{WT} + C_{SC} \tag{17}$$

Therefore the cost of the cooling system depends on the number of dry cells, n_{ACC}, the cost of each cell, C_{ACC}, the number of wet cooling towers, n_{WT}, the cost of each one, C_{WT} (see Table 7), and the cost of the surface condenser, C_{SC}. The cost of the latter depends on the contact surface area of this equipment, that depends on the number of tubes per tower and the number of towers. Following the model employed by Nithyanandam et al. [26], the cost of the heat exchanger, C_{SC}:

$$C_{SC} = 3.291 \cdot F_p \cdot F_l \cdot F_m \cdot exp(12.0310 - 0.8709\, log(A) + 0.0986\, ((log(A))^2)) \tag{18}$$

where F_p is the pressure factor, calculated using the maximum pressure in the condenser ($p_{max} = 60$ kPa), F_l is the tube length correction factor that is equal to 1, and F_m is the material factor, which can be calculated from: $F_m = a + (A/100)^b$, where a and b have been obtained from Seider et al. [27] and $A = \pi\, d_o\, L_s\, n_l\, n_{WT}$ (see Table 5). The investment costs

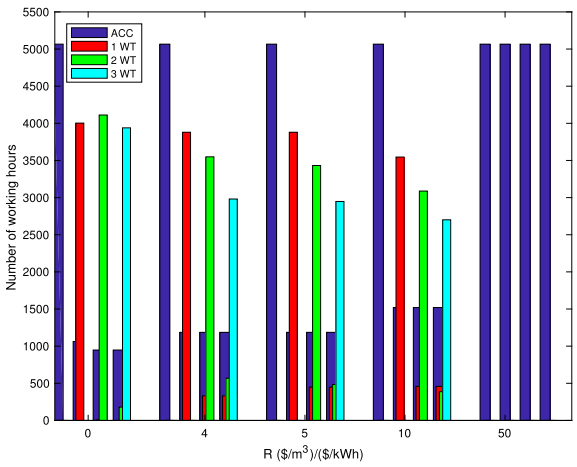

Fig. 10. Number of working hours of the dry and wet cooling tower as a function of the water to electricity price ratio, R. (a) 16 ACC, (b) 20 ACC (c) 24 ACC.

of the plant using this methodology is in agreement with the costs of the project of Shouhang Dunhuang in China [28–30].

The operation and maintenance costs include the labor costs, the maintenance of the equipment and the water consumption (see Eq. (19)).

$$C_{OM} = C_{labor}(n_{empl-plant} + n_{empl-SF}\, A_{SF}) + f_{OM} C_{invest} + m_{w,makeup}\, P_w \quad (19)$$

Table 7
Detailed costs of the plant. Prices have been updated to 2020 prices in dollars. The details of the calculation of investment costs are in appendix A.
Source: [1] Gómez-Hernández et al. [31], [2]NRE [32], [3] Turchi et al. [33], [4]Turchi and Heath [34], [5] Carapellucci and Giordano [35], [6] Ameri et al. [36], [7]Luceño and Martín [37], [8]Glatzmaier [38], [9] Panjeshahi et al. [39],[10], Stallings [40],[11]EIA [41], [12]Li et al. [42].

	Value
Solar subsystem, C_{solar} (M$)	348.03[1–8]
Power plant block*, C_{pp} (M$)	135.56[1–8]
Air cooled unit, C_{ACC} ($)	805.250[7]
Wet cooling tower, C_{WT} ($)	495.390[9,10]
Labor cost per employee and year ($/year)	48,000[5]
Number of employees (for plant operation), $n_{empl-SF}$	30[3]
Number of employees (field maintenance), $n_{empl-plant}$ (empl/m^2)	$2 \cdot 10^{-5}$ [5]
O&M operations, f_{OM} (%)	1[2]
–	–
Annual insurance cost, f_{ins} (%)	0.5[2,3]
Contingency cost, f_{cont} (%)	7[8]
Indirect cost, f_{ind} (%)	11[11]
Debt interest rate, i_{rate} (%)	8[2,3]
Inflation rate, f_{inf} (%)	3[12]
Lifetime (years), n_{yr}	30[2]

Another important economic indicator is the Total Net Present Value, TNPV, that measures the profitability of an investment: a positive TNPV indicates that the investment is viable. This parameter is the present value of the annual project after-tax cash flow. The total net present value is calculated as follows:

$$TNPV = \sum_{i=1}^{n_{yr}} \frac{B_i - C_i}{(1 + i_{rate})^i} \quad (20)$$

where B_i are the annual revenues of the plant, C_i the annual costs and i_{rate} is the discount rate.

The annual revenues, B_i of the plant can be calculated as the incomes due to the electricity sale and the income of carbon credits [43] (see Eq. (21)). China has recently launched a national carbon market with an initial price of carbon credit, $P_{CO_2} = 6.3$ $/ton that is expected to increase up to $P_{CO_2} = 21.4$ $/ton by 2050. Although the price of carbon credits is still uncertain, a linear increase in the price has been assumed for the present study.

$$B_i = E_{ann} \cdot P_e + E_{ann} \cdot CI \cdot P_{CO_2,i} \quad (21)$$

where CI is the carbon intensity emission factor of the grid $CI = 0.580$ ton/MWh [44].

The annual costs of a CSP plant, C_i, include the repayment of the loans, C_{loan}, the operation and maintenance costs, C_{OM}, and the tax costs, C_{tax}: $C_i = C_{loan,i} + C_{OM,i} + C_{tax,i}$. It can be assumed that the total investment costs, C_{invest}, are borrowed from banks and the repayment of the loans is done by even repayment schedule: $C_{loan,i} = C_{prin} + C_{int,i}$, where the principal, C_{prin} (the portion of the unpaid balance), is paid equally each year, while the payment of the interest, $C_{int,i}$, diminishes. For the current study the repayment period, n_{yr}, is the same as the expected lifetime of the power plant, so the principal can be calculated as: $C_{prin} = C_{invest}/n_{yr}$ and the interest on the year i:

$$C_{int,i} = (C_{invest} - (i-1)C_{prin}) \cdot i_{rate} \quad (22)$$

where an interest rate $i_{rate} = 0.08$ has been chosen [32].

The operation and maintenance costs increase year by year with inflation, $C_{OM,i} = C_{OM}(1 + f_{inf})^{(i-1)}$. Finally, in China for high-tech projects the income tax rate is 15%, and the depreciation and interest of loans can be excluded from the taxable income [42]. As proposed by Zhou et al. [43], double-declining balance depreciation method is employed to calculate the depreciation of the equipment assuming null salvage value at the end of the service period.

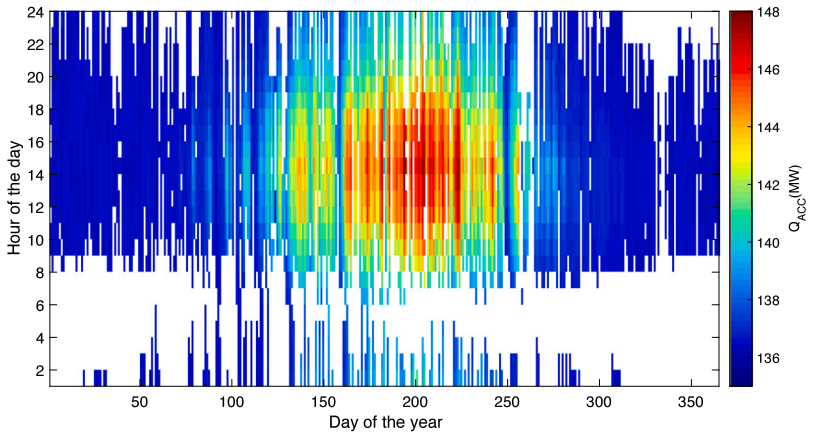

(a)

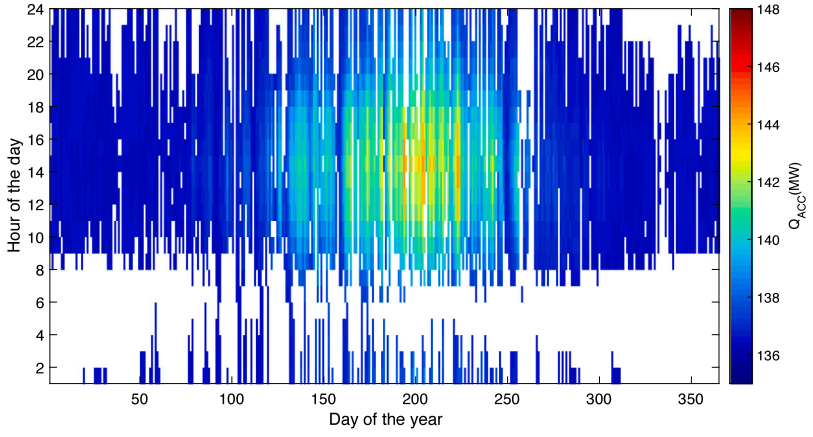

(b)

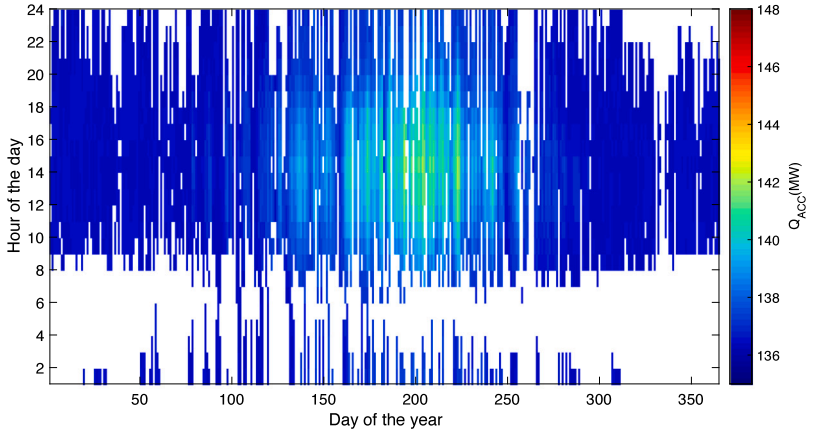

(c)

Fig. 11. Hourly distribution of the heat dissipated by the air condenser system: (a) 16 ACC (b) 20 ACC and (c) 24 ACC).

To compare among plants with dry and hybrid cooling systems the $LCOE$ and $TNPV$ are calculated for a plant with a dry condensing system with either 16, 20 or 24 ACC cells and a plant with hybrid condensing system with an additional wet part composed of either one, two or three cooling towers.

Concerning the results for the configuration with a dry air cooled system, Table 8 shows the total investment costs, the annual energy production, the capacity factor, which is the ratio of the net electricity generated to the energy that could have produced with continuous operation at nominal conditions for a period of time considered, and the LCOE. As expected, the investment costs, the annual energy yield and the capacity factor increase with the number of dry cooling units, since as the number of dry cooling tower increases the condensing temperature can be reduced and therefore the efficiency of the cycle and the power produced increases. It is interesting to notice that the increase in the annual energy production (and therefore in the capacity

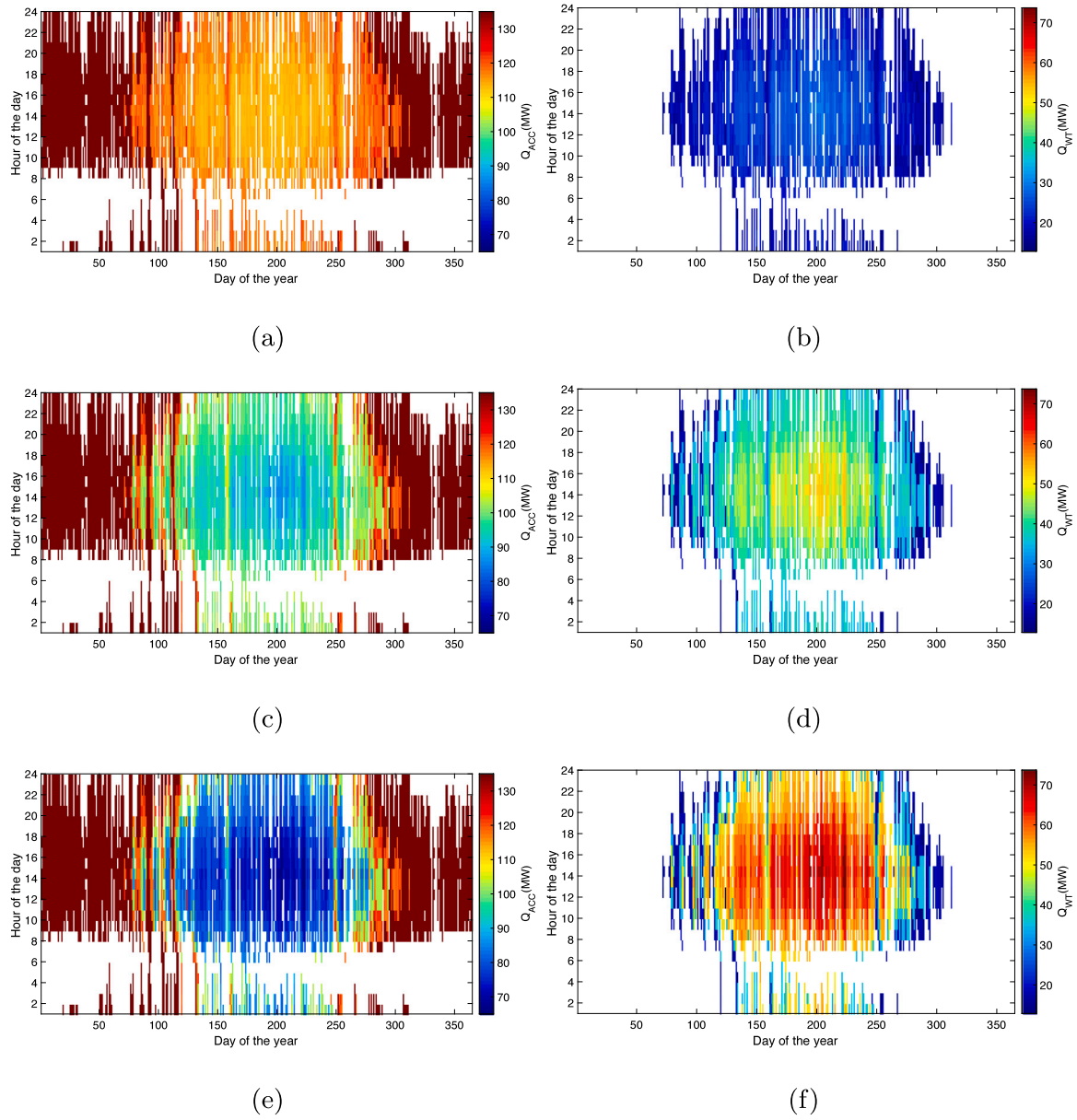

Fig. 12. Distribution of (a) heat rejected by ACC for 20 ACC + 1 WT system, (b) heat rejected by WT for 20 ACC + 1 WT system, (c) heat rejected by ACC for 20 ACC + 2 WT system, (d) heat rejected by WT for 20 ACC + 2 WT system, (e) heat rejected by ACC system for 20 ACC + 3 WT system, and (f) heat rejected by WT for 20 ACC + 3 WT system. All the cases shown in the figure correspond to a water-to-electricity price, R, of 10 ($/m^3)/($/kWh$_e$).

Table 8
Summary of the simulation results for the solar plant with different dry cooling systems.

Dry cooling units n_{ACC}	Investment costs C_{invest} (M$)	Annual energy yield E_{ann} (GWh)	Capacity factor CF	LCOE (c$/kWh$_e$)
16	589.73	533.78	0.609	11.94
20	593.55	538.98	0.615	11.90
24	597.38	541.24	0.618	11.93

factor) is not linear with the number of cooling units. Hence, for the case of Dunhuang the optimum dry cooling system is the system with 20 ACC units, since it has the lowest LCOE.

Table 9 shows the annual results of energy production, water consumption and CO_2 emissions avoided of the different configurations (including dry and hybrid) for different values of the ratio of water to energy price, R. The CO_2 emissions avoided by the CSP plant have been calculated multiplying the annual energy production by the carbon intensity emission of the grid CI = 0.580 ton/MWh [44]. As could be expected, for the dry condensing systems the water to energy price, R, has no effect on the annual energy yield, the emissions avoided or the water consumption, while for hybrid condensing systems as the water cost increases the annual energy production decreases, and in particular if the variable R = 50 ($/m^3)/($/kWh$_e$) the hybrid condensing system works as a dry system. Hence, the increase of the water cost discourages the start of the wet towers, and hence the water consumption is smaller at higher R for a given configuration. From another point of view, for a particular water to electricity price, R, with the exception of R = 50 ($/m^3)/($/kWh$_e$), increasing the number of wet towers increases the annual energy yield, water consumption and CO_2 emissions avoided. It is interesting to remark that the amount of CO_2 avoided increases with the number of ACC cells, and also increases when adding wet cooling towers to the cooling system while the water to electricity price has a minimum impact on this magnitude.

On one hand, increasing the number of wet towers increases the fixed and the operation costs, but on the other the annual energy yield

Table 9
Summary of simulation results for different water and electricity price ratio, R.

ACC	WT	Energy prod. (GWh/yr)	Water consump. (10^5 m^3/yr)	Avoided CO_2 (10^5 t/yr)	ACC	WT	Energy prod. (GWh/yr)	Water consump. (10^5 m^3/yr)	Avoided CO_2 (10^5 t/yr)	ACC	WT	Energy prod. (GWh/yr)	Water consump. (10^5 m^3/yr)	Avoided CO_2 (10^5 t/yr)
R = 0														
16	0	533.78	0	3.10	20	0	538.98	0	3.13	24	0	541.24	0	3.14
16	1	539.47	1.83	3.13	20	1	542.01	1.64	3.14	24	1	543.28	1.55	3.15
16	2	542.72	3.46	3.15	20	2	544.00	3.26	3.16	24	2	544.74	3.12	3.16
16	3	544.66	4.74	3.16	20	3	545.36	4.49	3.16	24	3	545.76	4.28	3.17
R = 4 [($/m^3)/($/kWh_e)]														
16	0	533.78	0	3.10	20	0	538.98	0	3.13	24	0	541.24	0	3.14
16	1	538.75	1.74	3.12	20	1	541.38	1.51	3.14	24	1	542.69	1.37	3.15
16	2	541.39	3.14	3.14	20	2	542.80	2.67	3.15	24	2	543.62	2.30	3.15
16	3	542.85	4.13	3.15	20	3	543.72	3.50	3.15	24	3	544.21	3.01	3.16
R = 5 [($/m^3)/($/kWh_e)]														
16	0	533.78	0	3.10	20	0	538.98	0	3.13	24	0	541.24	0	3.14
16	1	538.58	1.72	3.12	20	1	540.86	1.34	3.14	24	1	542.56	1.29	3.15
16	2	541.07	3.06	3.14	20	2	541.88	2.34	3.14	24	2	543.40	2.17	3.15
16	3	542.44	4.05	3.15	20	3	542.52	3.07	3.15	24	3	543.92	2.81	3.15
R = 10 [($/m^3)/($/kWh_e)]														
16	0	533.78	0	3.10	20	0	538.98	0	3.13	24	0	541.24	0	3.14
16	1	537.76	1.55	3.12	20	1	540.55	1.23	3.14	24	1	542.00	0.99	3.14
16	2	539.63	2.73	3.13	20	2	541.35	2.16	3.14	24	2	542.23	1.73	3.15
16	3	540.63	3.61	3.14	20	3	541.82	2.84	3.14	24	3	542.67	2.25	3.15
R = 50 [($/m^3)/($/kWh_e)]														
16	0	533.78	0	3.10	20	0	538.98	0	3.13	24	0	541.24	0	3.14
16	1	533.78	0	3.10	20	1	538.98	0	3.13	24	1	541.24	0	3.14
16	2	533.78	0	3.10	20	2	538.98	0	3.13	24	2	541.24	0	3.14
16	3	533.78	0	3.10	20	3	538.98	0	3.13	24	3	541.24	0	3.14

is also bigger. The water consumed has an effect on the $LCOE$ since it is part of the operation and maintenance cost of the plants that use cooling towers. This change of cost of the electricity resulting from the acquisition of wet towers and the water costs can be measured using $\Delta LCOE$ that takes into account the variation of the electricity costs due to the cooling system (see Eq. (23)). Negative $\Delta LCOE$ means that the costs to produce electricity are reduced and therefore that it is a cost-effective combination, while positive values of $\Delta LCOE$ mean that it is unprofitable.

$$\Delta LCOE = LCOE - LCOE_{ACC} \tag{23}$$

where $LCOE_{ACC}$ is the LCOE for the power plant using only dry units. $\Delta LCOE$ depends on the water price P_w, but also in the electricity price, P_e, since the operation strategy of the cooling system is to increase the net annual income of the power plant, hence it depends on the water to electricity price ratio, R. Fig. 13 shows the variation of the LCOE with the number of wet towers.

As it can be seen in Fig. 13 when the water price is null it is always advantageous the acquisition and use of hybrid systems compared to dry cooling systems. Furthermore, when $R = 0$ increasing the number of towers is always favorable, because the electricity cost decreases, although it decreases more slowly with the addition of each wet tower. Finally, it can be noticed that the smaller the dry system the bigger the reduction in the levelized cost of electricity. When the water to electricity price ratio, R, increases the use of hybrid systems becomes less cost-effective. For the case of the condensing system with fewer cells the use of hybrid condenser is always advantageous, however for $R = 10$ ($/m^3)/($/kWh$_e$) for the systems with 20 and 24 cells the water costs became too expensive to make the hybrid system profitable. For the case of 20 ACC and $R = 4$ ($/m^3)/($/kWh$_e$) the most profitable option is the use of 3 WT ($LCOE = 11.87$ c$/kWh$_e$) however if the water to electricity price increases to $R = 5$ ($/m^3)/($/kWh$_e$), then the most beneficial configuration is 1 single WT ($LCOE = 11.89$ c$/kWh$_e$). In Fig. 13, it can also be seen that for the 24 ACC system and $R = 4$ ($/m^3)/($/kWh$_e$) the smallest levelized cost of electricity is for 1 WT ($LCOE = 11.86$ c$/kWh$_e$) while the use of 3 WT is

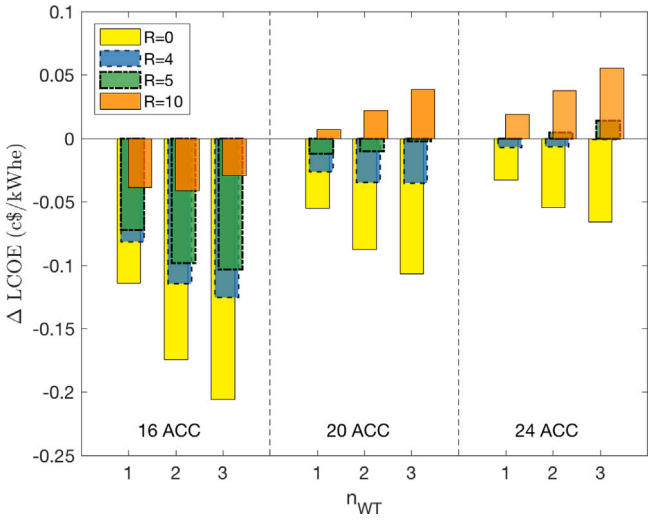

Fig. 13. Variation of LCOE with the cooling system.

disadvantageous because it has higher levelized costs of energy than using only dry condensers. Finally, for the 24 ACC system and $R = 5$ ($/m^3)/($/kWh$_e$), the LCOE of 1 WT is approximately equal to the use of only ACCs, and increasing the number of WT increases the LCOE.

Fig. 14 shows the variations of the TNPV with the number of cooling towers for different water to electricity price ratios for the total lifetime. It shows that all the configuration proposed: dry and hybrid are economically viable. Furthermore, in view of the results, the three dry cooling configurations (16, 20 and 24 ACC) are very similar, being the most profitable the 20 ACC system regardless of the water price. However for the hybrid systems, the most cost-effective configuration is the 16 ACC with 3 wet cooling towers for all water to electricity price ratio except for the $R = 10$ ($/m^3)/($/kWh$_e$) where the best option is

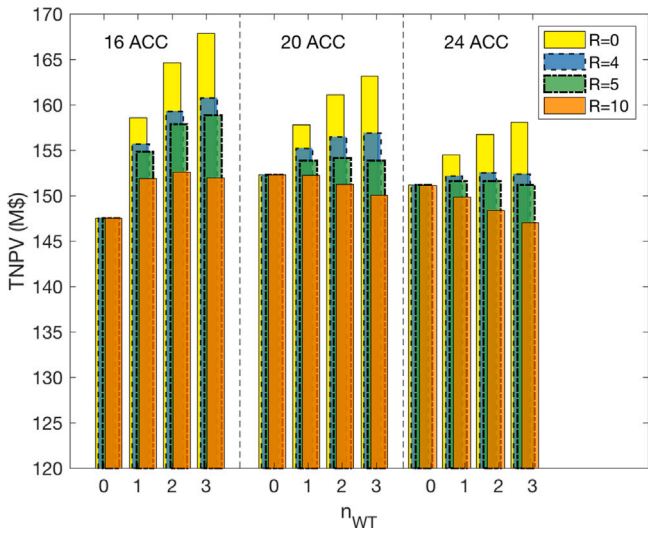

Fig. 14. Variations of TNPV with water-to-electricity price ratio for different cooling systems: 16 ACC (left), 20 ACC (center), 24 ACC (right).

with only 2 wet towers. As it could be expected, the higher the water to electricity price the less profitable become the wet towers.

4. Conclusion

A solar tower plant located at Dunhuang (China) was simulated to study the influence of the type of condensing system on the energy and economical performance. Dry systems of 16, 20 or 24 ACC cells and hybrid systems of 16, 20 or 24 ACC cells in parallel with a wet system of 1, 2 or 3 mechanical draft cooling tower units were analyzed. The selection of the operational parameters for the dry and wet systems was done with the aim of maximizing the revenues of the sale of the net energy produced minus the cost of the water consumed during the operation of the condensing system. This optimization gives, among other results, the proportion of the cooling load that is covered by the wet subsystem. At high dry-air and wet bulb temperatures, a higher proportion is recommended unless the water price to electricity price ratio is high in which case the higher cycle efficiency does not counterbalance the higher water cost incurred and hence it is better to switch off a certain number of cooling tower units.

Besides, the effect of the ambient dry and wet temperature on the heat dissipated by the condenser and the power consumed by the fan of a dry and a wet cooling systems was discussed. With this aim, simulations of each type of cooling subsystem (ACC, surface condenser and cooling tower) were done varying the inlet parameters. For the ACC, higher dry-air temperatures lead to a higher condensing temperature and hence lower cycle efficiency while the energy consumed by the fan is independent from the dry-air temperature and condensing temperature. Concerning the wet cooling system a higher rotational speed of the pump of the surface condenser leads to a lower condensation temperature but the fan power consumption augments.

The results of the annual simulation of the CSP plant located at Dunhuang reveals that for dry cooling systems, the number of ACC units does not change the energy performance during cold days. Nevertheless when ambient temperature increases, the smaller the condensation system, the higher the condensation heat rejected, since a system with a lower number of ACC units operates at higher condensation temperature and hence it has a lower cycle efficiency. On the other hand considering an hybrid system with 20 ACC units, having either one, two or three cooling tower units does not make a difference in the energy performance during cold days, since the wet part of the cooling system is switched off. However, during hot days the proportion of the condensing heat that is rejected by the cooling towers augments, from a 20% for a cooling system with only one wet cooling tower to a 50% for a system with three cooling towers.

Finally the LCOE and NPV of the CSP plant with different condensing system configurations were calculated and the system composed of 16 ACC cells and three wet cooling towers presents the lowest LCOE and highest NPV for a water to electricity price ratio of 4 or 5 while a system with 16 ACC cells and two wet cooling towers would the best option if this ratio is equal to 10.

Declaration of competing interest

The authors declare that they have no known competing financial interests or personal relationships that could have appeared to influence the work reported in this paper.

Acknowledgment

This research is partially funded by the Spanish government under the project RTI2018-096664-B-C21 (MICINN/FEDER, UE).

Appendix A

See Table A.10.

Appendix B. Notation

B.1. Acronyms

ACC	Air-cooled condenser
BOP	Balance of Plant
CSP	Concentrating solar energy
CT	Cold salt storage tank
DNI	Direct Normal Irradiation
HT	Hot salt storage tank
HPT	High pressure turbine
$LCOE$	Levelized cost of energy [c$/kWh$_e$]
LPT	Low pressure turbine
SC	Surface condenser
SG	Steam generator
PB	Power block
PH	Preheater
RH	Reheater
RC	Receiver
SH	Superheater
T	Turbine
$TNPV$	Total net present value [M$]
TOD	Time of delivery
WT	Wet cooling-tower

B.2. Latin letters

A	Heat transfer area [m^2]
A_c	Inside tube area exposed to the condensing steam for the each tube row of the air-cooled condenser [m^2]
A_e	Effective fan area [m^2], $A_e = \frac{\pi \cdot (d_F^2 - d_h^2)}{4}$
a_{fi}	Wetted area divided by the volume of the fill or area density [-]
A_{fr}	Effective frontal area of one bundle of the air-cooled condenser [m^2]
A_{Tfr}	Effective frontal area of the fill of the cooling tower [m^2]
A_{hel}	Heliostat area [m^2]
A_{SF}	Solar field area [m^2]
A_t	Surface condenser tube cross section [m^2]

Table A.10
Economic estimations ($) for different power plant components.

Component	Costs	Comments
Solar subsystem		
Solar Field	$C_{SF} = 140 \cdot n_{hel} \cdot A_{hel} + 16 \cdot A_{SF}$	A_{SF}: Solar field area (m^2) [33,45]
Solar Tower	$C_{tower} = 3 \cdot 10^7 + 1835.7 \cdot H_{tower}^2 - 285868 \cdot H_{tower}$	H_{tower}: Tower height (m)[33]
Receiver	$C_{rec} = 104.6 \cdot 10^6((\pi \cdot D_{rec} \cdot H_{rec})/1571)^{0.7}$	[46,47]
Storage system	$C_{st} = 22 \cdot 10^3 \cdot n_{st} \cdot Q_{in}$	[33]
Power block & Steam generators		
Steam turbine	$C_T = 5075.5 \cdot W_{PB}^{0.7}$ $(1 + \frac{0.05}{(1-\eta)^3}) \cdot (1 + 5(exp(\frac{T_{HPT}-866}{10.42})))$	W_{PB} Power block power (kW) T_{HPT}: Temperature (K) at the inlet of HPT [35]
Steam generator	$C_{SG} = 5.063 \cdot 10^6$	Superheater, reheater, evaporator and preheater [31]
Deaerator	$C_{dea} = 145315 \cdot m_{dea}^{0.7}$	m_{dea}: mass flow rate through deareator [36,48]
Feed water heater	$C_{FWH} = 66 \cdot Q_{FWH} \left(\frac{1}{T_{TTD}+a_3}\right)^{0.1}$	Q_{TTD}: Heat exchanged in FWH T_{TTD}: Terminal temperature difference $a_3 = 3$ for low pressure feed water heaters $a_3 = 6$ for high pressure feed water heaters
Water pump	$C_P = 1773 \cdot W_P^{0.7}$	W_P: Power of water pumps (kW) [31,48]
Buildings	$C_{buil} = 21 \cdot 10^6$	Buildings, structures support and fire protection [32]
Mechanical and electrical BOP		[32]
Power distribution system	$C_{e,sys} = 23 \cdot 10^6$	Power distribution system + Back-up + Instruments and Control System
Inflation costs	$C_{ST,BOP} = 20 \cdot 10^6$	
	$C_{2020} = C \cdot (1 + f_{inf,2020})$	$f_{inf,2020}$: inflation to year 2020.

a Surface area per unit volume [m^{-1}]
B Economic hourly revenue [$]
B_{Ti} Cooling tower breadth [m]
B_i Net annual income [-]
CI Carbon intensity emission factor [ton/MWh]
CR_{max} Maximum capacity rate [kg/s], $CR_{max} = max\left(\frac{\dot{m}_w c_{p,w}}{dh_{sat,w}/dT_w}, \dot{m}_a\right)$
CR_{min} Minimum capacity rate [kg/s], $CR_{min} = min\left(\frac{\dot{m}_w c_{p,w}}{dh_{sat,w}/dT_w}, \dot{m}_a\right)$
C_e Evaporative capacity rate ratio [-], $C_e = \frac{CR_{min}}{CR_{max}}$
C Cost [$]
c_p Specific heat [J/(kg K)]
d_e Hydraulic diameter [m]
d_h Fan hub diameter [m]
d_i Internal diameter [m]
d_o External diameter [m]
E Hourly energy [kWh$_e$]
E_{ann} Annual energy [kWh$_e$]
F_m Correction factor [-]
f Friction factor [-]
f_{cont} Contingency costs factor [-]
f_{cr} Capital recovery factor [-]
f_{ind} Indirect costs factor [-]
f_{inf} Inflation rate [-]
f_{ins} Insurance costs factor [-]
f_{OM} O&M costs factor [-]
G Mass velocity, [kg/s m^2]
g Gravity constant, 9.81 [m/s^2]
H_{dif} Diffuser height of the air-cooled condenser [m]
H_F Fan height of the cooling tower [m]
H_{fi} Height of the cooling tower fill [m], $H_{fi} = H_{Ti} + L_{fi} + L_{sp}$
H_{he} Height of the air-cooled condenser heat exchanger above ground level [m]
H_T Cooling tower height [m]
H_{Ti} Cooling tower inlet height [m]
$h_{ae}\,A_a$ Effective heat transfer coefficient from the air side for each tube row of the air-cooled condenser [W/K)]
h_c Condensation heat transfer coefficient from the steam side for each tube row of the air-cooled condenser [W/(m^2 K)]
h_d Mass transfer coefficient [kg/(m^2 s)]
h Specific enthalpy [J/(kg)]
i_r Interest rate [-]
K_{do} Total loss coefficient for flow obstacles at the fan discharge of the air-cooled condenser [-]
K_{ts} Heat exchanger inlet support loss coefficient of the air-cooled condenser [-]
K_{up} Total loss coefficient for flow obstacles at the fan suction of the air-cooled condenser [-]
K_{upfi} Fan upstream loss coefficient of the wet cooling tower [-]
$K_{\theta t}$ Total loss coefficient for the bundle with inlet and downstream losses due to oblique flow of the air-cooled condenser [-]
L_{fi} Fill height of the cooling tower [m]
L_{sp} Height of the spray zone of the cooling tower [m]
L_s Length of surface condenser tube [m]
L_t Length of air-cooled condenser finned tube [m]
Me Merkel number [-]
$\dot{m}$ Mass flow rate [kg/s]
N Rotational speed [-]
N_c Cycle of concentration [-]
NTU Number of transfer units [-], $NTU = \frac{U\,A}{C_{min}}$
n_{yr} Expected lifetime [year]
n_{ACC} Number of air-cooled condenser units [-]
n_b Number of air-cooled condenser tube bundles [-]
n_r Number of air-cooled condenser tube rows [-]
n_t Number of tubes per pass and tower [-]
n_{tb} Number of air-cooled condenser tubes per bundle [-]
n_{vp} Number of steam passes [-]
n_{wp} Number of cooling water passes [-]
n_{WT} Number of wet cooling tower units [-]
Q Heat rate [W]
P_{CO_2} Price of carbon credit [$/kWh$_e$]
P_e Electricity price [$/kWh]
P_w Water price [$/m^3]
p Internal pressure [MPa]
R Water to electricity price ratio[($/m^3)/($/kWh$_e$)]
Re Reynolds number [-]
th Tube thickness [m]
T Temperature [°C]
U Overall heat transfer coefficient [W/(m^2 K)]
V Volume flow rate [m^3/s]
W Electrical power [W]
W_{Ti} Cooling tower inlet width [m]
X Vapor quality at the outlet of the turbine [-]

B.3. Greek symbols

λ Correction factor [-], $\lambda = \left(h_{sat,w,o} + h_{sat,w,i} - 2\,h_{sat,w}\right)$
ε Effectiveness [-]
η Efficiency [-]
θ Apex angle of V-frame of air-cooled condenser [°]
ρ Density [kg/m^3]
ω Humidity ratio [-]

B.4. Subscripts

a Air
av Average air-vapor
c Condensing
dea Deaerator
ev Evaporation
F Fan
Fr Reference fan
fi Fill
FWH Feedwater heater
hel Heliostat
i Inlet
o Outlet
io Average inlet–outlet
P Pump
rec Receiver
ref Reference
rz Rain zone
sat Saturation temperature
sp Spray zone
w Cooling water

References

[1] C. Turchi, M. Wagner, C. Kutscher, Water Use in Parabolic Trough Power Plants: Summary Results from Worley Parsons' Analyses, NREL Technical Report, 2010, NREL/TP-5500-49468, URL: http://www.nrel.gov/docs/fy11osti/49468.pdf.

[2] F. Asfand, P. Palenzuela, L. Roca, A. Caron, C.A. Lemarié, J. Gillard, P. Turner, K. Patchigolla, Thermodynamic performance and water consumption of hybrid cooling system configurations for concentrated solar power plants, Sustainability 12 (2020) 4739.

[3] C.S. Turchi, M.J. Wagner, C.F. Kutscher, Water Use in Parabolic Trough Power Plants: Summary Results from Worley Parsons' Analyses, Technical Report, National Renewable Energy Lab. (NREL), 2010.

[4] M.J. Wagner, C.F. Kutscher, Assesing the impact of heat rejection technology on CSP plant revenue, in: Proceedings of the SolarPACES 2010, Perpignan, France, September 21-24, 2010.

[5] T.E. Boukelia, A. Bouraoui, A. Laouuafi, S. Djimli, Y. Kabar, 3E (Energy-Exergy-Economic) comparative study of integrating wet and dry cooling systems in solar tower power plants, Energy 200 (2020) 117567.

[6] R.B. Boulay, M.J. Cerha, M. Massoudi, Dry and hibrid condenser cooling design to maximize operating income, in: Proceedings of PWR2005, ASME Power, Chicago, IllinoisUSA, 2005.

[7] C. Marugán-Cruz, S. Sánchez-Delgado, J. Gómez-Hernández, D. Santana, Towards zero water consumption in solar tower power plants, Appl. Therm. Eng. 178 (May) (2020) 115505, URL: https://doi.org/10.1016/j.applthermaleng.2020.115505, http://dx.doi.org/10.1016/j.applthermaleng.2020.115505.

[8] S. Rohani, J. Went, D.F. Duvenhage, R. Gerards, C. Wittwer, T. Fluri, Optimization of water management plans for CSP plants through simulation of water consumption and cost treatment based on operational data, Sol. Energy 223 (2021) 278–292.

[9] FluxSPT software tool, 2017, http://ise.uc3~m.es/research/solar-energy/fluxspt, Accessed: 2021-07-19.

[10] SolarPILOT software tool, 2020, https://www.nrel.gov/csp/solarpilot.html, Accessed: 2021-01-19.

[11] M.J. Wagner, Simulation and Predictive Performance Modeling of Utility-Scale Central Receiver System Power Plants (Ph.D. thesis), University Of Wisconsin, 2008.

[12] PVGIS, Photovoltaic geographical information system, 2021, http://re.jrc.ec.europa.eu/pvg_tools/en/tools.html, Accessed: 2021-12-16.

[13] M.R. Rodríguez-Sánchez, A. Sánchez-González, C. Marugán-Cruz, D. Santana, Flow patterns of external solar receivers, Sol. Energy 122 (2015) 940–953.

[14] A.B. Zavoico, Solar Power Tower: Design Basis Document, 2001, Report No. SAND2001-2100, Alburquerque, NM, USA.

[15] R.C. Spencer, K.C. Cotton, C.N. Cannon, A method for predicting performance of steam generators:. 16,500 kW and larger, J. Eng. Power 4 (1963) 249–298.

[16] R. Srinivasan, Optimum condenser cooling water temperature rise in power plants, in: ASME(Ed.), Proceedings of IJPGC03, 2003, pp. 15–29.

[17] D.G. Kroger, Air-Cooled Heat Exchangers and Cooling Towers, vol. 2, PennWell, 2004.

[18] M.S. Bhatti, R.K. Shah, Urbulent and transition convective heat transfer in ducts, in: Handbook of Single-Phase Convective Heat Transfer (Ch. 4), John Wiley & Sons, Inc., 1987.

[19] Standards for Steam Surface Condensers, Technical Report, Heat Exchange Institute, 2012.

[20] J. Saari, J. Kaikko, E. Vakkilainen, S. Savilainen, Comparison of power plant steam condenser heat transfer models foron-line condition monitoring, Appl. Therm. Eng. 62 (2014) 37–47.

[21] D.G. Kroger, Air-Cooled Heat Exchangers and Cooling Towers, vol. 1, PennWell, 2004.

[22] J.M. Douglas, Conceptual Design of Chemical Process, Mc-Graw Hill, New York, USA, 1988.

[23] J.R. Singham, Heat Exchanger Design Handbook, Hemisphere Publishing Corporation, New York, USA, 1983.

[24] H.E. Beck, N.E. Zimmermann, T.R. McVicar, N. Vergopolan, A. Berg, E.F. Wood, Present and future Köppen-Geiger climate classification maps at 1-km resolution, Sci. Data 5 (2018) 180214, URL: http://dx.doi.org/10.1038/sdata.2018.214.

[25] J. Aldersey-Williams, T. Rubert, Levelised cost of energy - A theoretical justification and critical assessment, Energy Policy 124 (2018) (2019) 169–179, URL: http://dx.doi.org/10.1016/j.enpol.2018.10.004, http://dx.doi.org/10.1016/j.enpol.2018.10.004.

[26] K. Nithyanandam, P. Shoaei, R. Pitchumani, Technoeconomic analysis of thermoelectric power plant condensers with nonwetting surfaces, Energy 227 (2021) 120450.

[27] W.D. Seider, D.R. Lewin, J.D. Seder, S. Widagdo, R. Gani, K. Ming Ng, Product and process design principles, in: Synthesis, Analysis and Evaluation, Wiley, 2017, p. 725.

[28] J. Lilliestam, M. Labordena, A. Patt, S. Pfenninger, Empirically observed learning rates for concentrating solar power and their responses to regime change, Nat. Energy 2 (7) (2017) http://dx.doi.org/10.1038/nenergy.2017.94.

[29] J. Lilliestam, R. Pitz-Paal, Concentrating solar power for less than USD 0.07 per kWh: finally the breakthrough? Renew. Energy Focus 26 (00) (2018) 17–21, URL: http://dx.doi.org/10.1016/j.ref.2018.06.002, http://dx.doi.org/10.1016/j.ref.2018.06.002.

[30] J. Lilliestam, R. Thonig, C. Zang, A. Gilmanova, CSP.guru, 2021, https://www.csp.guru, Accessed: 2021-07-01.

[31] J. Gómez-Hernández, P.A. González-Gómez, J. Briongos, D. Santana, Maximizing the power block efficiency of solar tower plants: Dual-pressure level steam generator, Appl. Therm. Eng. 144 (2018) 583–592.

[32] NREL, System advisor model (SAM): CSP cost data, 2020, https://sam.nrel.gov/concentrating-solar-power/csp-cost-data.html, Accessed: 2021-07-22.

[33] C.S. Turchi, M. Boyd, D. Kesseli, P. Kurup, M. Mehos, T. Neises, P. Sharan, M.J. Wagner, T. Wendelin, CSP Systems Analysis - Final Project Report CSP Systems Analysis - Final Project Report, 2019.

[34] C.S. Turchi, G.A. Heath, Molten Salt Power Tower Cost Model for the System Advisor Model (SAM), NREL Technical Report, NREL/TP-5500-57625, 2012.

[35] R. Carapellucci, L. Giordano, A comparison between exergetic and economic criteria for optimizing the heat recovery steam generators of gas-steam power plants, Energy 58 (2013) 458–472, URL: http://dx.doi.org/10.1016/j.energy.2013.05.003, http://dx.doi.org/10.1016/j.energy.2013.05.003.

[36] M. Ameri, P. Ahmadi, A. Hamidi, Energy, exergy and exergoeconomic analysis of a steam power plant: A case study, Int. J. Energy Res. 33 (2009) 499–512.

[37] J.A. Luceño, M. Martín, Two-step optimization procedure for the conceptual design of A-frame systems for solar power plants, Energy 165 (2018) 483–500.

[38] G. Glatzmaier, Developing a Cost Model and Methodology to Estimate Capital Costs for Thermal Energy Storage, NREL, 2011, NREL/TP-5500-53066.

[39] M.H. Panjeshahi, A. Ataei, M. Gharaie, R. Parand, Optimum design of cooling water systems for energy and water conservation, Chem. Eng. Res. Des. 87 (2) (2009) 200–209, http://dx.doi.org/10.1016/j.cherd.2008.08.004.

[40] J. Stallings, Economic Evaluation of Alternative Cooling Technologies, Technical Report, EPRI, 2012.

[41] IEA, Capital Cost Estimates for Utility Scale Electricity Generating Plants, Technical Report February, U.S. Energy Information Administration. U.S. Department of Energy, 2020, Accessed: 2021-05-08.

[42] W. Li, P. Wei, X. Zhou, A cost-benefit analysis of power generation from commercial reinforced concrete solar chimney power plant, Energy Convers. Manage. 79 (2014) 104–113, URL: http://dx.doi.org/10.1016/j.enconman.2013.11.046, http://dx.doi.org/10.1016/j.enconman.2013.11.046.

[43] X. Zhou, J. Yang, F. Wang, B. Xiao, Economic analysis of power generation from floating solar chimney power plant, Renew. Sustain. Energy Rev. 13 (4) (2009) 736–749, http://dx.doi.org/10.1016/j.rser.2008.02.011.

[44] IEA, Electricity Market Report, Technical Report February, IEA. International Energy Agency, 2020, http://dx.doi.org/10.1787/f0aed4e6-en.

[45] E. Casati, F. Casella, P. Colonna, Design of CSP plants with optimally operated thermal storage, Sol. Energy 116 (2015) 371–387, URL: http://dx.doi.org/10.1016/j.solener.2015.03.048, http://dx.doi.org/10.1016/j.solener.2015.03.048.

[46] G. Augsburger, Thermodynamic and Economic Assessment of a New Generation of Subcritical and Supercritical Solar Power Towers (Ph.D. thesis), École Polytechnique Fédérale de Lausanne, 2013, http://dx.doi.org/10.5075/epfl-thesis-5648.

[47] M.R. Rodríguez-Sánchez, A. Sánchez-González, P.A. González-Gómez, C. Marugán-Cruz, D. Santana, Thermodynamic and economic assessment of a new generation of subcritical and supercritical solar power towers, Energy 118 (2017) 534–544, http://dx.doi.org/10.1016/j.energy.2016.10.079.

[48] A.M. Elsafi, Exergy and exergoeconomic analysis of sustainable direct steam generation solar power plants, Energy Convers. Manage. 103 (2018) 338–347, URL: http://dx.doi.org/10.1016/j.enconman.2015.06.066, http://dx.doi.org/10.1016/j.enconman.2015.06.066.